Document made available under the Patent Cooperation Treaty (PCT)

International application number: PCT/US05/007649

International filing date: 10 March 2005 (10.03.2005)

Document type: Certified copy of priority document

Document details: Country/Office: US
Number: 60/551,816
Filing date: 10 March 2004 (10.03.2004)

Date of receipt at the International Bureau: 09 May 2005 (09.05.2005)

Remark: Priority document submitted or transmitted to the International Bureau in compliance with Rule 17.1(a) or (b)

1314030

THE UNITED STATES OF AMERICA

TO ALL TO WHOM THESE PRESENTS SHALL COME:

UNITED STATES DEPARTMENT OF COMMERCE

United States Patent and Trademark Office

April 26, 2005

THIS IS TO CERTIFY THAT ANNEXED HERETO IS A TRUE COPY FROM THE RECORDS OF THE UNITED STATES PATENT AND TRADEMARK OFFICE OF THOSE PAPERS OF THE BELOW IDENTIFIED PATENT APPLICATION THAT MET THE REQUIREMENTS TO BE GRANTED A FILING DATE.

APPLICATION NUMBER: *60/551,816*
FILING DATE: *March 10, 2004*
RELATED PCT APPLICATION NUMBER: *PCT/US05/07649*

Certified by

Jon W. Dudas

Under Secretary of Commerce
for Intellectual Property
and Director of the United States
Patent and Trademark Office

Please Type a plus sign (+) inside this box → +

2PTO/SB/16 (02/01)
Approved for use through 10/31/2002. OMB 0651-0032
U.S Patent and Trademark Office: U.S. DEPARTMENT OF COMMERCE

Under the Paperwork Reduction Act of 1995, no persons are required to respond to a collection of information unless it displays a valid OMB control number

PROVISIONAL APPLICATION FOR PATENT COVER SHEET

This is a request for filing a PROVISIONAL APPLICATION FOR PATENT under 37 CFR 1.53(c)

Express Mail Label No.: EV 415945538 US

INVENTOR(S)		
Given Name (first and middle [if any])	Family Name or Surname	Residence (City and either State or Foreign Country)
ROBERT MARTIN	DICKSON	ATLANTA, GEORGIA USA
JIE	ZHENG	ATLANTA, GEORGIA USA

☐ *Additional Inventors are being named on the 1 separately numbered sheets attached hereto.*

TITLE OF THE INVENTION (280 characters max)

DNA TEMPLATED Ag NANOCLUSTER FORMATION

CORRESPONDENCE ADDRESS

☐ Customer Number or Bar Code Label | (Insert Customer No. or Attach bar code label here) | Or ☒ Correspondence address below

NAME	**Office of Technology Licensing Georgia Tech Research Corporation Attention: Director**				
ADDRESS	**505 Tenth Street, NW**				
CITY	**Atlanta**	STATE	**Georgia**	ZIP CODE	**30332-0415**
COUNTRY	**U.S.A.**	TELEPHONE	**404-894-6287**	FAX	**404-894-9728**

ENCLOSED APPLICATION PARTS (*check all that apply*)

☒ Specification *Number of Pages* 43 ☐ CD(s), Number _____

☐ Drawing(s) *Number of Pages* _____ ☒ Other (Specify) Return postcard

☒ Application Data Sheet. See 37 CFR 1.76.

METHOD OF PAYMENT OF FILING FEES FOR THIS PROVISIONAL APPLICATION FOR PATENT

☒ Applicant claims small entity status. See 37 CFR 1.27

☐ A check or money order is enclosed to cover the filing fees

☒ The commissioner is hereby authorized to charge filing fees or credit any overpayment to Deposit Account Number: **502064**

☐ Payment by credit card. Form PTO-2038 is attached.

FILING FEE AMOUNT ($): 80.00

This invention was made by an agency of the United States government or under a contract with an agency of the United States Government.

☐ No.

☒ Yes, the name of the U.S. Government agency and the Government contact number are: NIH – contract no. 1 R01 GM68732-01; National Science Foundation – contract no. BES-0323453

Respectfully submitted,
GEORGIA TECH RESEARCH CORPORATION

SIGNATURE: Kimberly A. Dunn

TYPE or PRINTED NAME: Kimberly A. Dunn, Patent Coordinator

Date: March 10, 2004, 2002

Docket No.: 2704PR2

REGISTRATION NO.:

USE ONLY FOR FILING A PROVISIONAL APPLICATION FOR PATENT

This collection of information is required by 37 CFR 1.51. The information is used by the public to file (and by the PTO to process) a provisional application. Confidentiality is governed by 35 USC 122 and 37 CFR 1.14. This collection is estimated to take 8 hours to complete, including gathering, preparing, and submitting the complete provisional application to the PTO. Time will vary depending upon the individual case. Any comments on the amount of time you require to complete this form and/or suggestions for reducing this burden, should be sent to the Chief Information Office, U.S. Patent and Trademark Office, U.S. Department of Commerce, Washington, D.C. 20231. DO NOT SEND FEES OR COMPLETED FORMS TO THIS ADDRESS. SEND TO: Box Provisional Application, Assistant Commissioner for Patents, Washington, D.C. 20231.

PATENTS
IN THE UNITED STATES PATENT AND TRADEMARK OFFICE

In re application of: DICKSON, et al.

For: ***DNA Templated Ag Nanocluster Formation***

CERTIFICATE OF EXPRESS MAIL
FOR PROVISIONAL APPLICATION

Assistant Commissioner for Patents
Box PROVISIONAL PATENT APPLICATION
Washington, D.C. 20231

Sir:

Enclosed for filing in the above case are the following documents:

Provisional Application Patent Cover Sheet
Provisional Application
Fee Transmittal Form
Provisional Application Filing Fee, Small Entity - $80.00
Return Postcard

Respectfully submitted,

Kimberly A. Dunn
Patent Coordinator

GEORGIA TECH RESEARCH CORPORATION
OFFICE OF TECHNOLOGY LICENSING
505 Tenth Street, NW
Atlanta, Georgia 30332-0415

Our Reference No: **2704PR2**

I hereby certify that all correspondences listed above are being deposited for delivery to the above addressee, with the United States Postal Service **"EXPRESS MAIL POST OFFICE TO ADDRESSEE"** service under 37 CFR §1.10 on the date indicated below:

The envelope has been given U.S. Postal Service "Express Mail Post Office To Addressee" Package **# EV 415945538 U.S.**

3/10/04
Date

Kimberly Dunn

DNA Templated Ag Nanocluster Formation

Jeffrey T. Petty[#,*], Jie Zheng, Nicholas V. Hud, and Robert M. Dickson*

School of Chemistry and Biochemistry, Georgia Institute of Technology, Atlanta, GA 30332-0400

*E-mail: dickson@chemistry.gatech.edu, jeff.petty@furman.edu

[#]Permanent address: Department of Chemistry, Furman University, Greenville, SC 29613

Abstract

The high affinity of Ag^+ for DNA bases has enabled creation of short oligonucleotide-encapsulated Ag nanoclusters without formation of large nanoparticles. Time dependent formation of cluster sizes ranging from Ag_1 to Ag_4 /oligonucleotide were observed with strong, characteristic electronic transitions between 400 and 600 nm. The slow nanocluster formation kinetics enables observation of specific aqueous nanocluster absorptions that evolve over a period of 12 hrs. Induced circular dichroism bands confirm that the nanoclusters are associated with the chiral ss-DNA template. Fluorescence, absorption, mass, and NMR spectra all indicate that multiple species are present, but that their creation is both nucleotide and time-dependent.

Introduction

As bulk metals are devoid of a bandgap, metal nanoclusters must be extremely small to exhibit discrete electronic transitions and strong fluorescence. The change in optical, magnetic, electronic, and catalytic properties with size have therefore motivated many studies of metal nanoparticles.[1,2,3] These small particles with 1-100 nm diameters are produced via the reduction of metal cations, and their rate of growth is controlled using ligands that coordinate with the metal atoms.[4] Surfactants, thiols, amines, carboxylic acids and even dendrimers are all quite useful to bind, stabilize, concentrate, and direct growth of metal nanoparticles. Recently, poly(amidoamine) dendrimers (PAMAM) have been shown to stabilize even smaller Ag and Au nanoclusters with well-defined sizes while the surrounding polymeric matrix protects the developing nanoclusters against agglomeration following reduction.[3] Biological macromolecules have also served as templates for nanoparticle synthesis. For example, the amine functional groups of peptides assemble silver and gold cations and then cap the growing nanoparticle surface following reduction of the cations.[5] Another biological system of significant interest has been DNA because its large aspect ratio (length:diameter) allows the possibility of forming wires for use in nanoelectronics.[6] DNA has a high affinity for metal cations, and these localized cations can be reduced to form metallic nanoparticles that follow the contour of the DNA template.[6,7,8]

One reason for controlling the size of metal nanoparticles is to understand and utilize the strong size dependence of their electronic/optical properties.[1] We are particularly interested in the strong, size-dependent optical properties of small (2-8 atom) Ag nanoclusters. Along the atom to bulk transition,

discrete atomic energy levels merge into highly polarizable, continuous, plasmon-supporting bands. When sufficiently small, silver nanoclusters exhibit very strong absorption and emission, making them nearly ideal fluorophores for single molecule spectroscopy. Photochemically generated nanoclusters have strong fluorescence, and they can be optically interrogated, suggesting potential utility in high-density optical data storage[9] and as biological labels.[10] In this work, we utilize specific DNA-Ag interactions to further concentrate and narrow the Ag nanocluster distributions in aqueous solutions. The fine control of nanocluster size possible in DNA, its sequence specificity, and its potential to pattern materials on surfaces suggest many further uses ranging from biology to nanoscience.

Experimental

Silver nitrate (Aldrich, 99.998%) and sodium borohydride (Fisher, 98%) were used as received. Oligonucleotides (Integrated DNA Technologies) were purified by desalting by the manufacturer. The 12-base oligonucleotide 5'-AGGTCGCCGCCC-3' was received as dehydrated pellets and dissolved in a 5 mM phosphate buffer (pH = 7.5). This oligonucleotide sequence was used as it favors the single-stranded vs. hairpin or self-dimer forms. Concentrations were based on the nearest neighbor approximations for the molar absorptivities. Reactions were conducted in either 5 mM phosphate or 100 mM $NaClO_4$ /5 mM phosphate buffer.[11] The silver nanoclusters were synthesized by first cooling the solution of DNA and Ag^+ to 0 °C and then adding $NaBH_4$ followed by vigorous shaking.

Visible absorption spectra were acquired using a Shimadzu UV-2101PC spectrometer. Circular dichroism spectra were obtained from a Jasco J-710 spectropolarimeter. Fluorescence spectra were acquired on a Shimadzu RF-5301PC spectrofluorimeter. Mass spectra were acquired using a Micromass Quattro LC operated in negative ion mode with 2.5 kV needle and 40 V cone voltages. NMR spectra were acquired on a Bruker DRX 500 operating at 500 MHz.

Results and Discussion

Base Association

Ag^+ strongly favors association with the heterocyclic bases and not the phosphates.[12,13] Supporting evidence comes from spectroscopic shifts for the Ag^+-laden DNA complexes, the insensitivity of the affinity to competing cations, and the higher affinity for single-stranded vs. double-stranded DNA.[14,15] Thermodynamic measurements indicate at least two modes of binding.[15,16] For Ag^+:base concentrations < 0.2, complexes form with the purines via nitrogen or π-electron coordination. For higher silver concentrations (0.2 < Ag^+:base < 0.5), a weaker complex forms and involves coordination with the nitrogens of either the purines or pyrimidines. In our studies, we also find changes in the electronic absorption and circular dichroism spectra that indicate the silver ions and nanoclusters associate with the bases. For the 12-base oligonucleotide, the DNA absorption maximum (λ_{max}) shifts from 257 nm to 267 nm upon Ag^+ complexation (1 Ag^+:2 bases) (Fig. 1). Following reduction of the bound ions, further spectral changes occur. Initially, λ_{max} shifts from 267 nm to 256 nm, and the molar absorptivity increases. This latter effect may be attributed to new, overlapping electronic bands for small silver clusters, which are

known to absorb in this spectral region.[17] Alternatively, the dipole coupling between the excited electronic states of the bases could be altered by structural changes induced by the silver nanoclusters, a possibility also suggested by the circular dichroism spectra (vide infra). Eventually, as Ag nanoclusters grow and visible absorptions evolve (vide infra), the λ_{max} shifts to 262 nm and the molar absorptivity decreases.

The electronic transition of the bases exhibit a small circular dichroism (CD) due to the chirality of the riboses, and this spectroscopic technique is sensitive to the arrangement of the bases.[18] For the Ag^+ complex with double-stranded DNA, circular and linear dichroism studies show that Ag^+ induces nonplanar and tilted orientations of the bases relative to the helical axis.[11] For the single-stranded oligonucleotide, we observe CD spectra that are similar to those for double-stranded DNA, suggesting that Ag^+ may cause similar perturbation of the bases in single-stranded DNA (Fig. 2). Analogous to the evolution of the absorption spectra (Fig. 1), the CD spectra also change upon reduction of the Ag^+. The differences between the spectra in Fig. 2 indicate that the silver nanoclusters induce different structural changes in DNA than does Ag^+.

Nanocluster Sizes

Because of the monodispersity of synthesized DNA oligonucleotides, the stoichiometry of the nanoclusters can be accurately determined using electrospray mass spectrometry (Fig. 3). These experiments were conducted in water to reduce the concentrations of cations that would form adducts with the DNA and consequently reduce sensitivity. The experiments also used a higher concentration of oligonucleotide (75 μM) to enhance the ion abundance. In Fig. 3A, the dominant peak in the spectrum occurs at 3607 amu, as expected for the 12 base oligonucleotide. Addition of 6 Ag^+:oligonucleotide (1 Ag^+:2 bases) results in complexes with a maximum of 4 Ag^+ per DNA strand. This difference between the total and bound ion concentrations may be attributed to the weaker adducts that form at higher silver concentrations,[15] which may be more susceptible to dissociation during desolvation and/or ionization. A poor description of the ion intensities is observed when they are fit as a Poisson distribution, which suggests that 4 Ag^+/oligonucleotide is the favored stoichiometry (Fig. 3A). The DNA sequence used for these studies favors the single-stranded form as opposed to self-duplex or hairpin forms. The mass spectra indicate that the clusters are also bound to a single DNA strand. Following reduction of the bound Ag^+ ions, the number of bound silver atoms is initially small, but the distribution shifts to higher stoichiometries with time (Fig. 3B). As opposed to the Ag^+ complexes, a Poisson distribution gives a more accurate description of the ion distributions for the reduced complexes. The following average cluster sizes were measured: 1.8 ± 0.3 (50 mins), 2.4 ± 0.2 (350 min), and 3.0 ± 0.2 (1050 min). The observed distribution terminates at 4 Ag/oligonucleotide, which again differs from a Poisson distribution. End effects may contribute to the stoichiometries of both the ion and metal complexes with these short oligonucleotides, but spectroscopic studies directly suggest that the base sequence is a significant feature of the interaction of the nanoclusters with DNA (vide infra). The mass spectra do not distinguish the possibility of single clusters or multiple smaller clusters bound to a single oligonucleotide, and studies with oligonucleotides of varying lengths and sequences may resolve this issue.

Nanocluster Spectra

Mass spectrometry demonstrates that a small number (≤ 4) of silver atoms are bound to the single-stranded DNA template, and the following spectroscopic studies demonstrate that these silver atoms form nanoclusters. Reduction of the Ag^+ bound to the DNA results in new species with electronic transitions in the visible region of the spectrum (Fig. 4). The transition that is most prominent initially has a λ_{max} = 426 nm at 9 min after adding the BH_4^-. Over a period of 12 hours, the absorbance of this band decreases and a broad absorption band with peaks at 424 and 520 nm develops. As determined through theoretical and low temperature spectroscopic studies, electronic transitions for small silver clusters, in particular Ag_2 and Ag_3, are expected in this spectral region.[17,19,20] Using these prior studies, a definitive assignment of the electronic bands is problematic because the peaks for the DNA-bound cluster are expected to shift and broaden relative to their gas-phase and rare gas matrix-isolated values. No change in the absorbances or peak positions is observed when the solutions are centrifuged, indicating that the spectra cannot be attributed to nanoparticles. Similar spectra are observed when 2 BH_4^-:1 Ag^+ is used, indicating that the spectra arise from fully reduced silver clusters (not shown). In a buffer with 100 mM $NaClO_4$, the results are similar to those in the lower salt buffer, with the only difference being a broad band without distinct peaks after longer times. This similarity suggests nanocluster formation is not impeded by competing cations, which is consistent with their association via the bases and not the phosphates.

Because the small silver clusters do not have inherent chirality, the induced CD associated with the Ag nanocluster electronic transitions is further evidence that the clusters are bound to the DNA (Fig. 5). The most prominent band has a minimum response at 440 nm and this minimum shifts to longer wavelengths with time. However, unlike the absorption spectra, the magnitude of this response does not diminish with time. A shoulder at 500 nm suggests the species that contribute to the longer wavelength absorptions (Fig. 4) are also bound to the DNA strand.

As opposed to larger metal nanoparticles, a distinctive feature of small nanoclusters is their strong fluorescence due to their lower density of electronic states. For the DNA bound nanoclusters, prominent fluorescence is observed at ≈ 630 nm (Fig. 6). For excitation between 240 and 300 nm, a band at 630 nm is observed with the maximum intensity observed using 260 nm excitation. While this result suggests the cluster emission occurs via energy transfer, the silver clusters also have higher lying excited states accessible in this spectral region. Thus, emission following direct excitation of the higher electronic bands of the silver clusters is also feasible.

The multiple peaks in the absorption and circular dichroism spectra suggest the presence of small clusters with varying stoichiometries. The fluorescence spectra provide further evidence that the samples contain multiple species, but the mass spectra indicate that each DNA strand encapsulates only a single Ag nanocluster. First, the maximum emission intensity (λ_{max} = 638 nm) occurs with an excitation wavelength of 560 nm (Fig. 6), which is significantly red-shifted relative to the absorption maximum at 520 (Fig. 4). Second, for excitation at wavelengths greater than 500 nm, the wavelength of maximum emission shifts to longer wavelengths as the excitation wavelength increases. One possibility suggested by Fig. 6 is that the emission band for the 560 nm excitation can be spectrally decomposed as the emission bands for 540 and 580 nm excitation. In other words, at least two distinct species contribute to the fluorescence in this wavelength region.

As suggested by the absorption spectra, NMR spectra also indicate that the silver nanoclusters interact directly with the DNA bases. The aromatic proton resonances in the ^{1}H NMR spectra of the oligonucleotide are well resolved prior to the addition of Ag^+ (Fig 7). However, the proton resonances are essentially broadened to baseline upon addition of Ag^+ (spectrum not shown). In contrast, most of the aromatic proton resonances in the ^{1}H spectra with silver clusters are almost as narrow as those of the free oligonucleotide (Fig. 7). The cytosine H6 proton resonances exhibit the largest change in chemical shift in the presence of the silver nanoclusters (Fig. 7). Similar upfield chemical shift changes were also observed for the H5 protons of cytosine (spectrum not shown). These observations indicate that the cytosine bases are most favored for interaction with the silver nanoclusters. The six cytosine H6 resonances were identified in 1D spectra based upon their splitting due to H6-H5 coupling, and by H6-H5 crosspeaks in 2D COSY spectra. However, it was not possible to determine the sequence position of each cystosine resonance in the proton spectrum. Nevertheless, the different chemical shift changes exhibited by the cytosine H6 resonances indicate that cytosine bases interact with silver clusters in a sequence-dependent manner. Experiments with additional oligonucleotide sequences are necessary to properly assess the relative association of adenine and thymine for silver nanoclusters.

Concentration Studies

To investigate the importance of the relative Ag^+:DNA stoichiometry, a 10 μM concentration of each oligonucleotide was maintained while the Ag^+ concentration was reduced from 1 Ag^+:2 bases (Fig. 4) to 1 Ag^+:10 bases (Fig. 8) and the cell pathlength was increased five-fold. While the two sets of spectra are similar with respect to the overall absorbances and the wavelengths of the transitions, differences are observed. The maximum absorbance for the 420 nm peak occurred at 20 min for the more dilute sample, or about twice as long as for the more concentrated sample (Fig. 4). This slower rate is expected when intermolecular exchange results in the formation of specific and favored cluster stoichiometries. The width of the 440 nm band is much narrower in the more dilute sample as opposed to the more concentrated sample, which suggests that a range of binding sites with slightly different electronic effects are available for binding by the silver clusters. At the lower concentration, the more favored sites are occupied, leading to an overall narrowing of the spectral transition. Another difference is the presence of a new band at 360 nm, and we observe no fluorescence associated with this band. No differences were observed in the fluorescence spectra of the concentrated and dilute samples.

Conclusions

Small (< 10 atoms) metallic nanoclusters have interesting optical properties and many potential applications, and we are interested in controlling their stoichiometry and thus, their optical and electronic properties. Toward this goal, we have utilized DNA templates for synthesizing silver nanoclusters. From this work, we reach the major conclusions that DNA acts as a template for the time-dependent and size-specific formation of nanoclusters. Prior to reduction, the Ag^+ ions have a strong interaction with the DNA strands. Then, addition of $NaBH_4$ results in 1 – 4 Ag atoms bound to the 12 base oligonucleotide, as determined through mass spectral analysis. The new electronic transitions that are observed in the absorption and fluorescence spectra are in the expected range for small silver nanoclusters. Base specific interactions could be a significant feature of these nanoclusters, as suggested from the chemical shifts in the

NMR spectra for the cytosine bases and the truncated distribution in the mass spectra. Together, these results suggest that it may be feasible to control the formation of nanoclusters with specific stoichiometries using DNA strands with specific sequences.

Acknowledgements

We appreciate the discussions with and the support of the following people: Q. Darugar, S. Jain, S. Kanvah, U. Santhosh, and G. B. Schuster. J. P. gratefully acknowledges the support provided by the Research Site for Undergraduate Educators. R. M. D. thanks Olympus America Inc. for equipment loan, and funding from the National Institutes of Health (1R01GM068731), the National Science Foundation (BES-0323453), the Vassar-Wooley, Dreyfus, and Sloan Foundations, the Blanchard Endowment for junior faculty, and the Center for Advanced Research in Optical Microscopy at Georgia Institute of Technology.

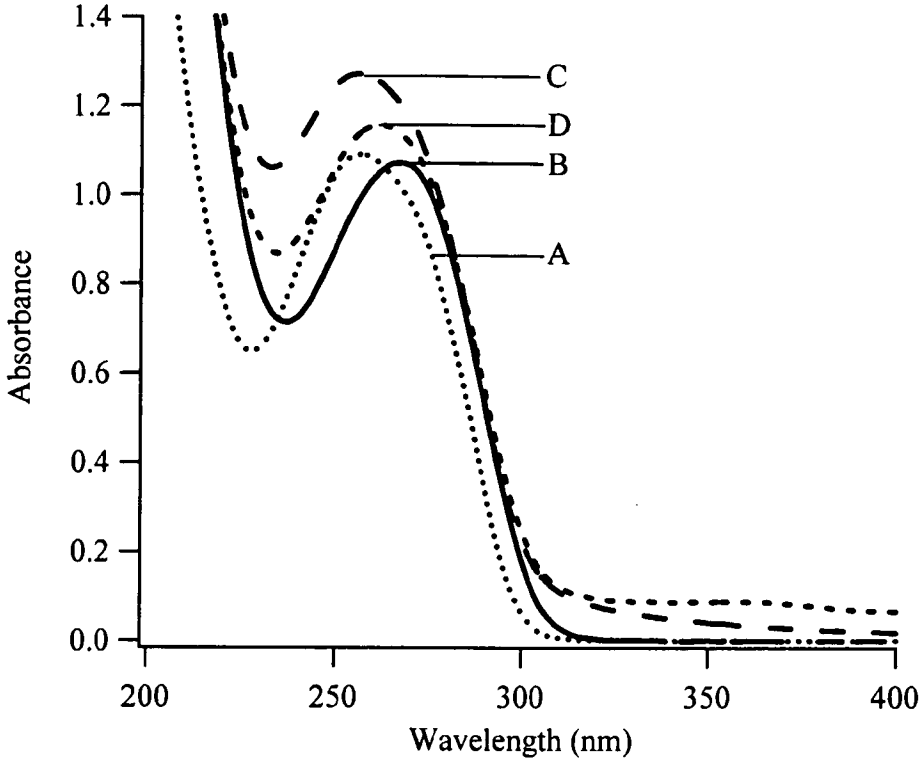

Fig 1. Response of the electronic transition of the oligonucleotide bases to association with Ag^+ and Ag nanoclusters. Following are the conditions for the spectra: A (dotted line) - 10 μM oligonucleotide solution; B (solid line) – oligonucleotide with 60 μM Ag^+ (1 Ag^+:2 bases); C (coarse dashed line) – 2 min. after adding 1 BH_4^-:1 Ag^+ to the oligonucleotide/Ag^+ solution; D (fine dashed line) - 1100 min after adding BH_4^- to the oligonucleotide/Ag^+ solution.

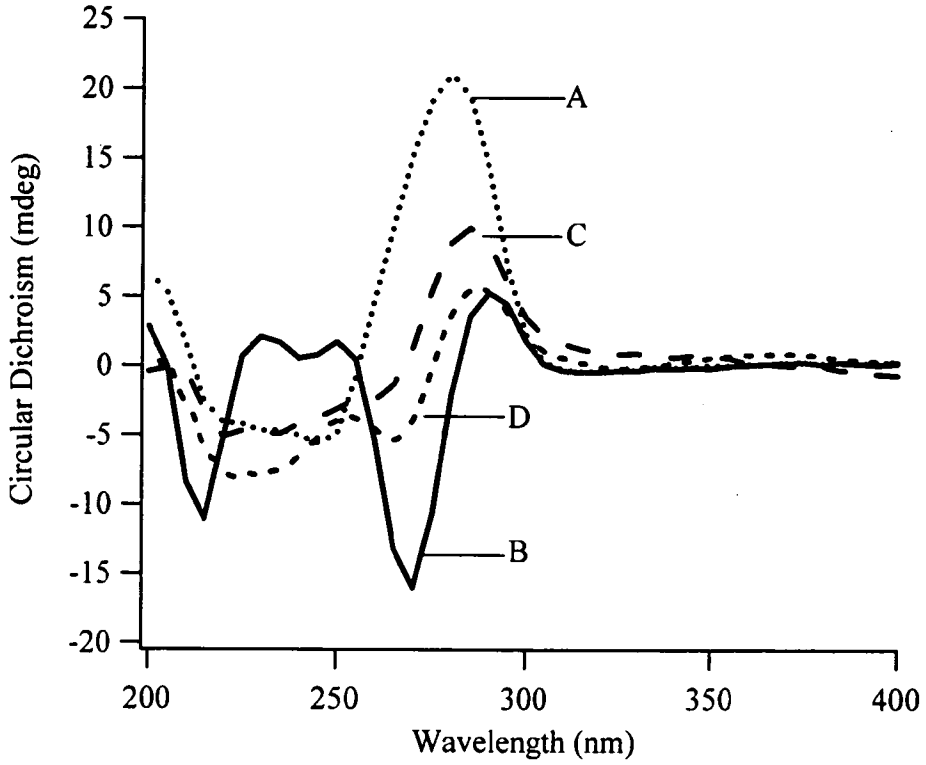

Fig. 2. Response of the circular dichroism associated with electronic transition of the oligonucleotide bases to association with Ag^+ and Ag nanoclusters. Following are the conditions for the spectra: A (dotted line) - 10 μM oligonucleotide solution; B (solid line) – oligonucleotide with 60 μM Ag^+ (1 Ag^+:2 bases); C (coarse dashed line) – 120 min. after adding 1 BH_4^-:1 Ag^+ to the oligonucleotide/Ag^+ solution; D (fine dashed line) - 4300 min after adding BH_4^- to the oligonucleotide/Ag^+ solution.

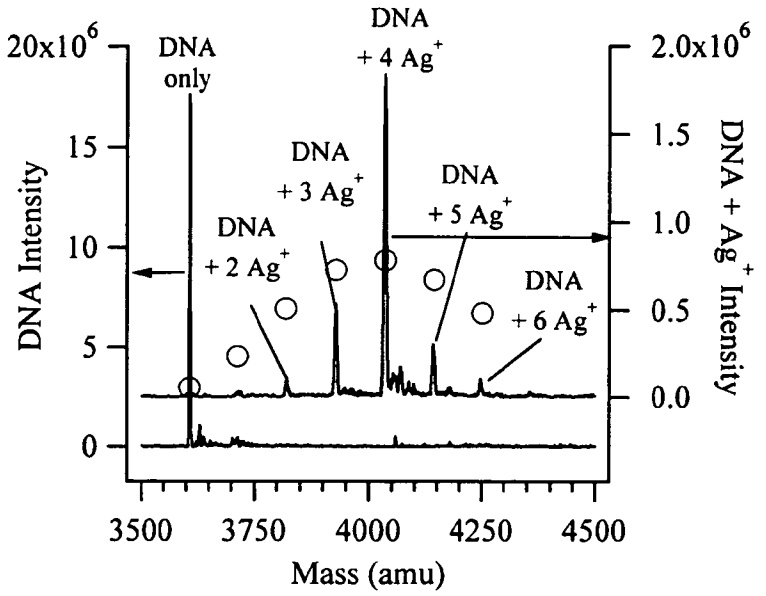

Fig. 3a Electrospray ionization mass spectra of the oligonucletide and silver ion adducts. Following are the conditions for the spectra: Left axis - 75 μM oligonucleotide solution with a peak at 3607 amu; Right axis – 75 μM oligonucleotide with 60 μM Ag^+ (1 Ag^+:2 bases) with peaks at 3821, 3928, 4035, 4141, and 4247 amu. The intensities of the peaks for the Ag^+/DNA complexes were fit with a Poisson distribution (open circles) to give a mean size of 4.3 ± 1.3 Ag^+/oligonucleotide.

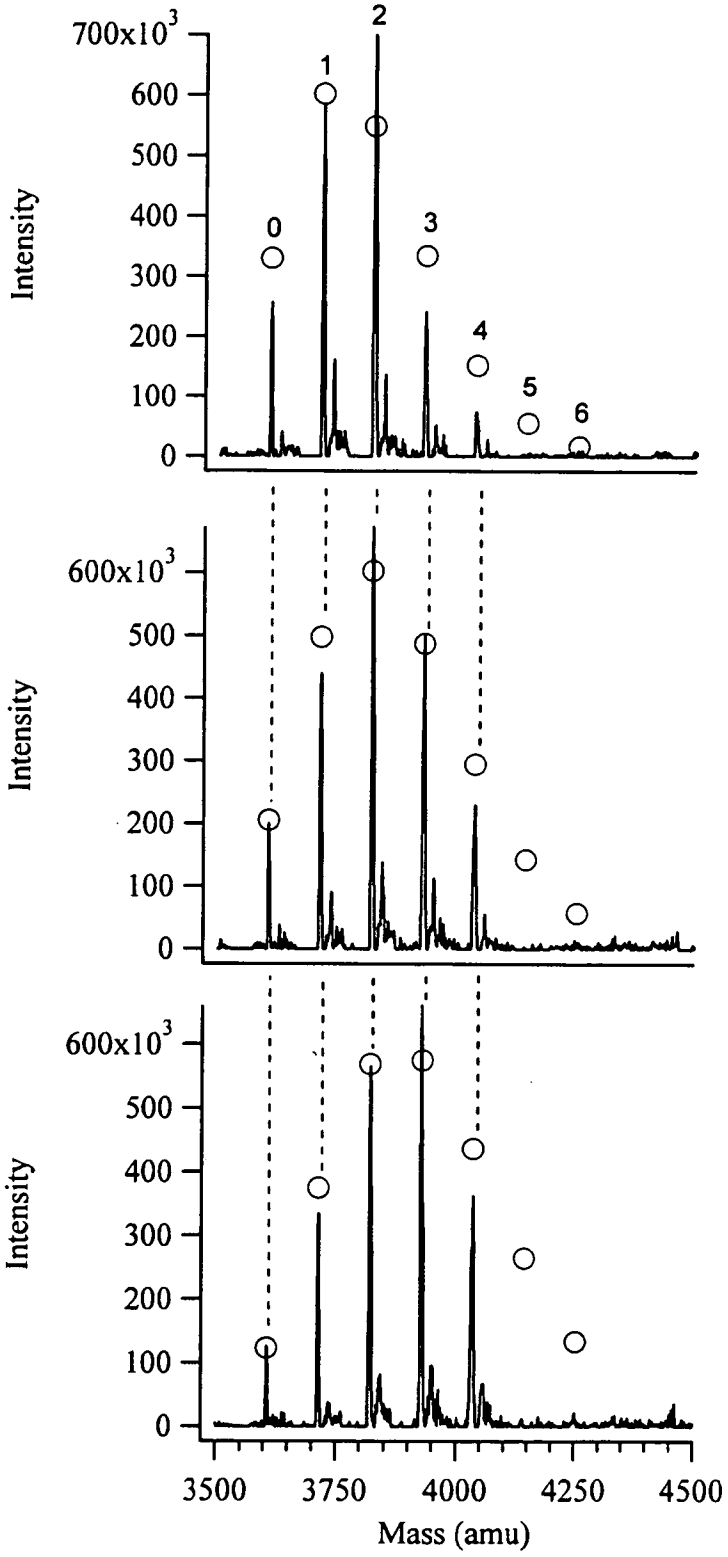

Fig. 3b Electrospray ionization mass spectra of silver cluster complexes with the DNA oligonucleotide. Overlaid as open circles are the Poisson fits of the intensity distributions and the mean number of bound Ag is provided in the parentheses. Following are the conditions for the spectra: Top – 75 μM oligonucleotide with 60 μM Ag^+ and 50 min. after adding 1 BH_4^-:1 Ag^+ (1.8 ± 0.3 Ag) Middle - 350 min after adding BH_4^- to the oligonucleotide/Ag^+ solution (2.4 ± 0.2 Ag); Bottom - 1050 min after adding BH_4^- to the oligonucleotide/Ag^+ solution (3.0 ± 0.2 Ag). The peaks are observed at 3607, 3714, 3821, 3927, and 4036 amu. The small peaks displaced by 22 amu are attributed to Na-DNA adducts due to the use of $NaBH_4^-$ for the reduction.

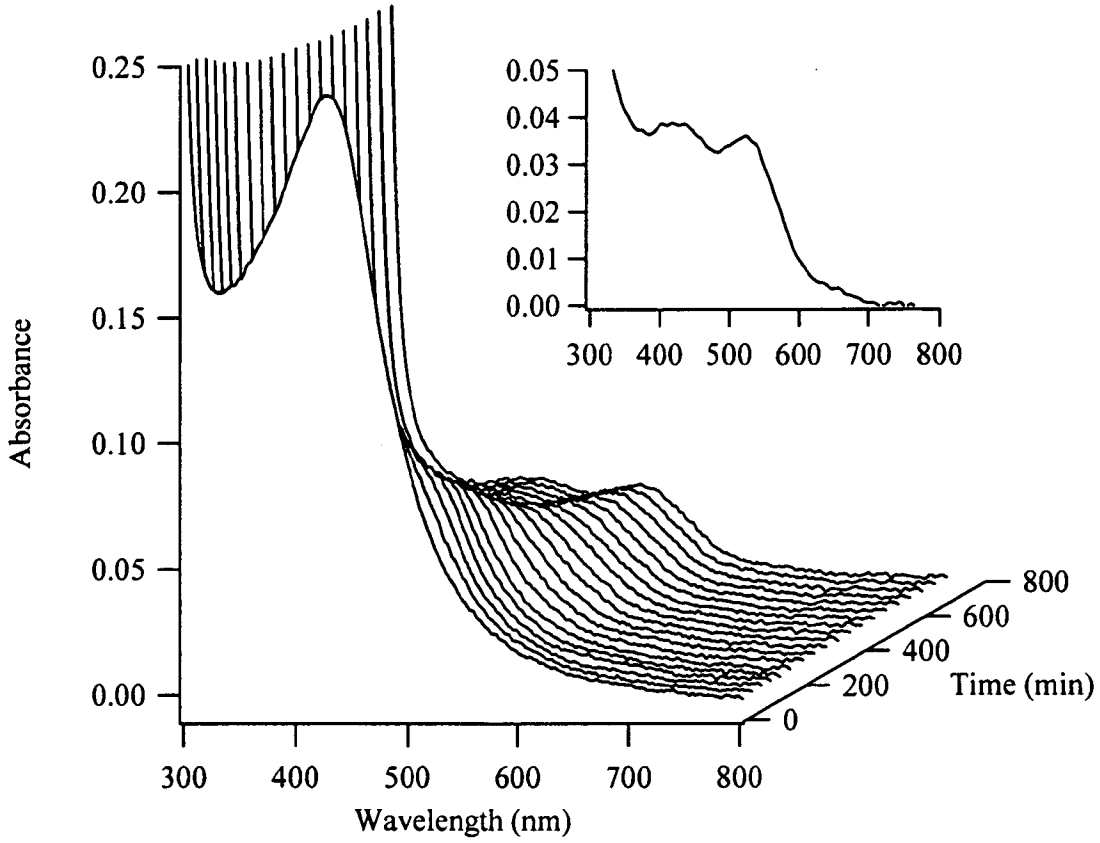

Fig 4. Absorption spectra associated with the DNA-bound silver nanoclusters . For these spectra, [oligonucleotide] = 10 μM, $[Ag^+]$ = 60 μM, and $[BH_4^-]$ = 60 μM. The foremost spectrum in the time series was acquired 9 mins after adding the BH_4^-, and it has λ_{max} = 426 nm. Subsequent spectra were acquired approximately every 30 mins. The inset spectrum shows the last spectrum in the series (692 mins) and peaks are observed at 424 and 520 nm.

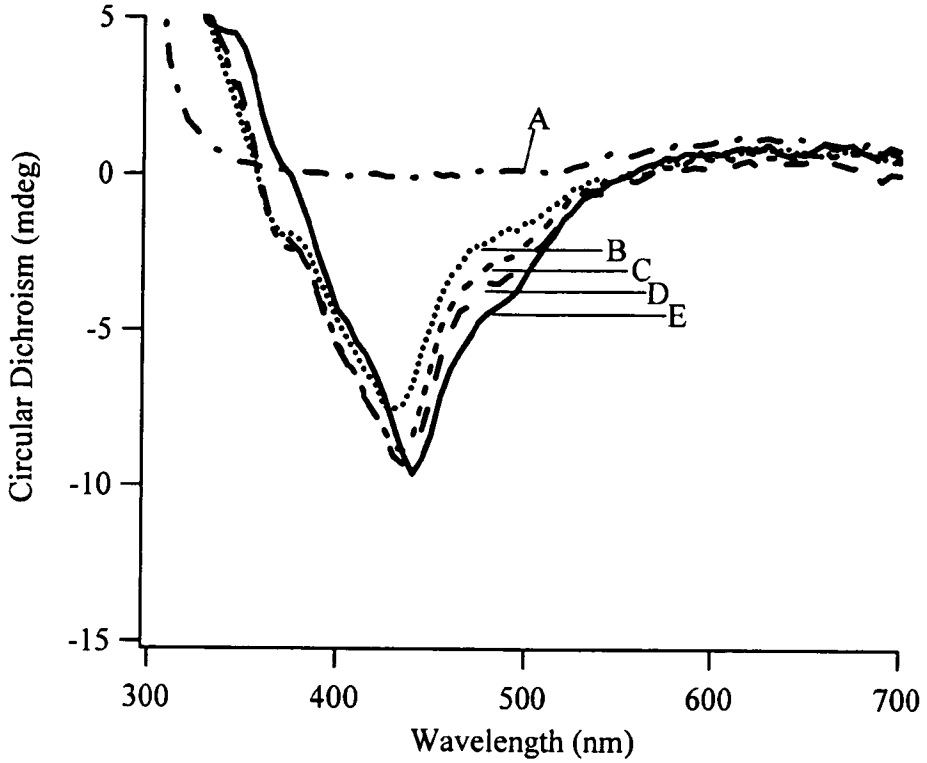

Fig. 5. Induced circular dichroism spectra for the electronic transitions associated with the nanoclusters. For these spectra, [oligonucleotide] = 10 μM, $[Ag^+]$ = 60 μM, and $[BH_4^-]$ = 60 μM in a 1 mM phosphate buffer and the cell pathlength was 5 cm. The spectra were collected 2 min (A – dashed-dotted line), 20 min (B – dotted line), 40 min (C – fine dashed line), 60 min (D – coarse dotted line), and 150 mins (E – solid line) after adding the BH_4^-.

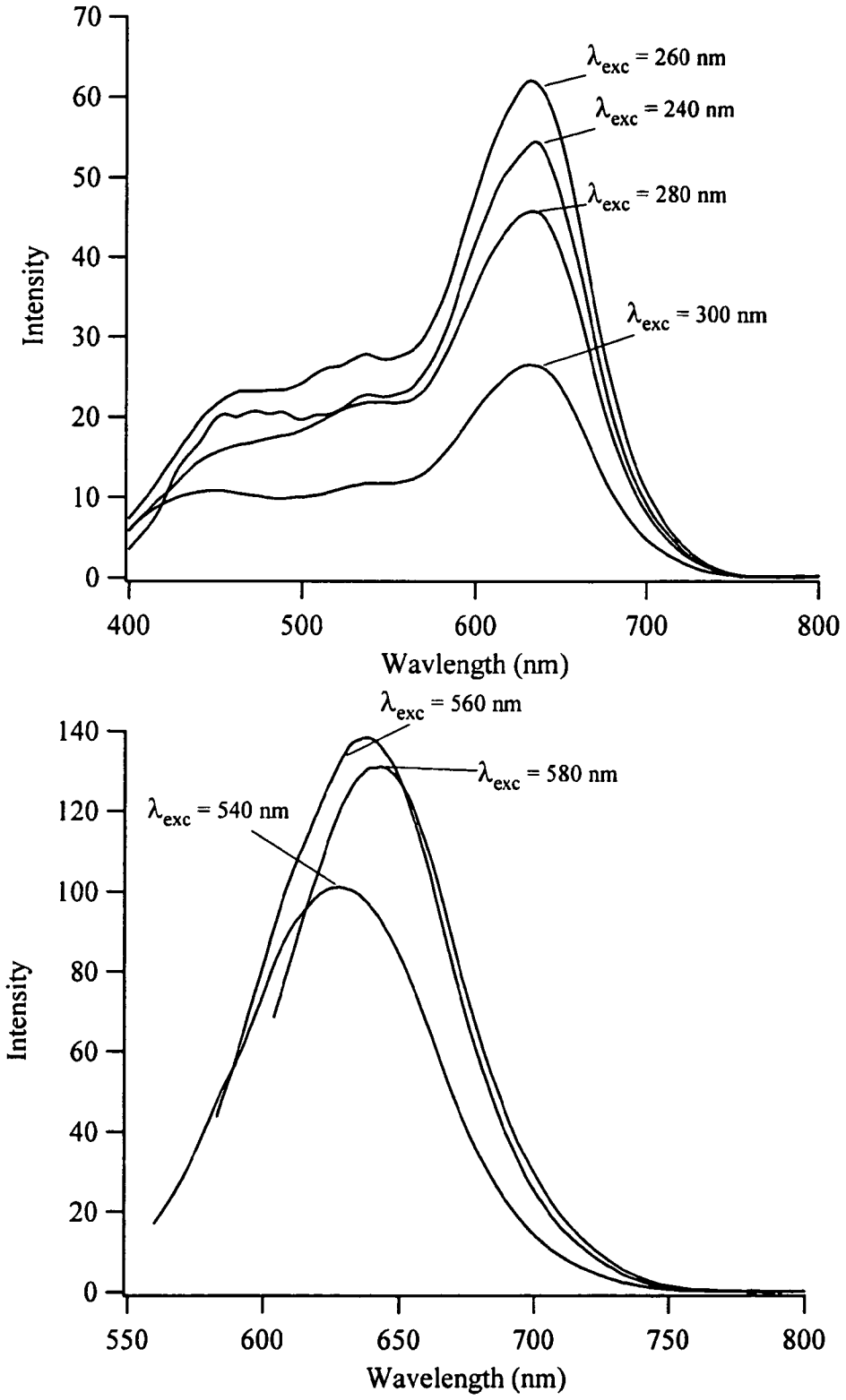

Fig. 6 Fluorescence emission spectrum of the silver nanoclusters bound to the oligonucleotide. For these spectra, [oligonucleotide] = 10 μM, [Ag^+] = 60 μM, and [BH_4^-] = 60 μM. In the top graph, a series of emission spectra were acquired using 240, 260, 280, and 300 nm excitation. A broad emission band is observed between 400 and 550 nm and a peak is observed at 632 nm. In the bottom graph, excitation at 540, 560, and 580 nm results in emission bands with maxima at 629, 638, and 642 nm, respectively.

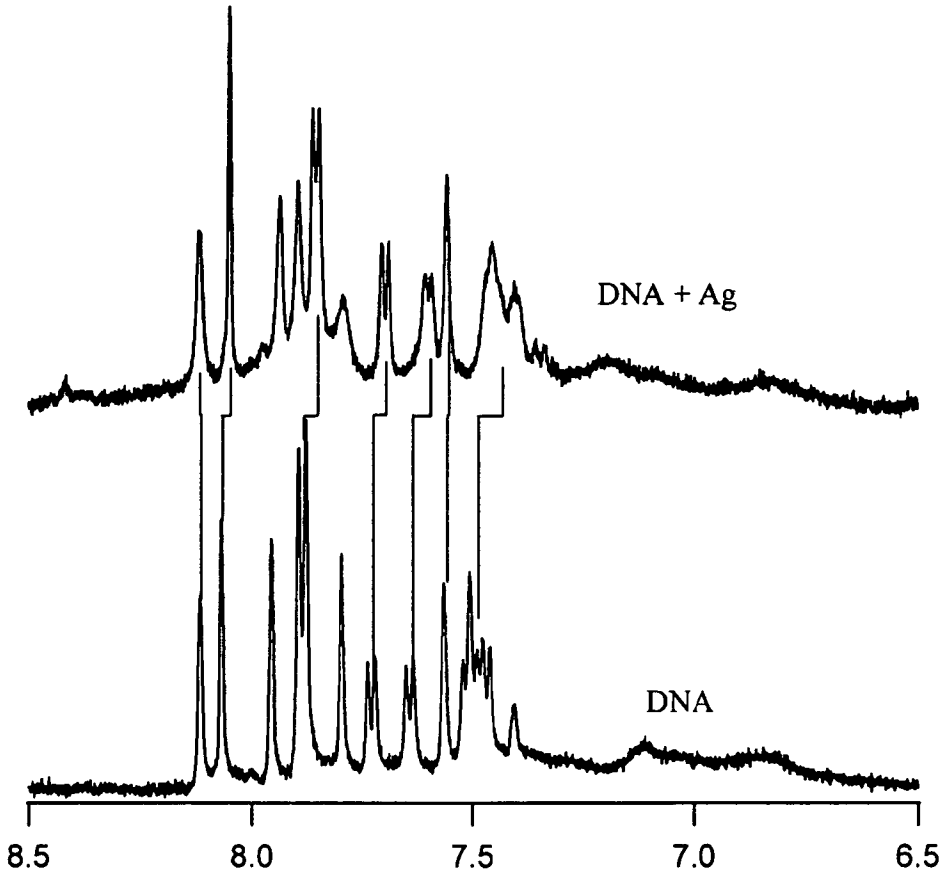

Fig 7. The aromatic proton region from ^{1}H NMR spectra of the oligonucleotide with and without the silver nanoclusters. Vertical lines indicate aromatic proton resonances with chemical shifts that change after nanocluster formation. Cytosine H6 resonances, which exhibit the largest changes in chemical shift, can be identified by their splitting due to coupling to cytosine H5. For these spectra, [oligonucleotide] = 0.93 mM, $[Ag^+]$ = 5.6 mM, and $[BH_4^-]$ = 5.6 mM in a solution of 90% 1 mM phosphate buffer and 10% D_2O at 25 °C.

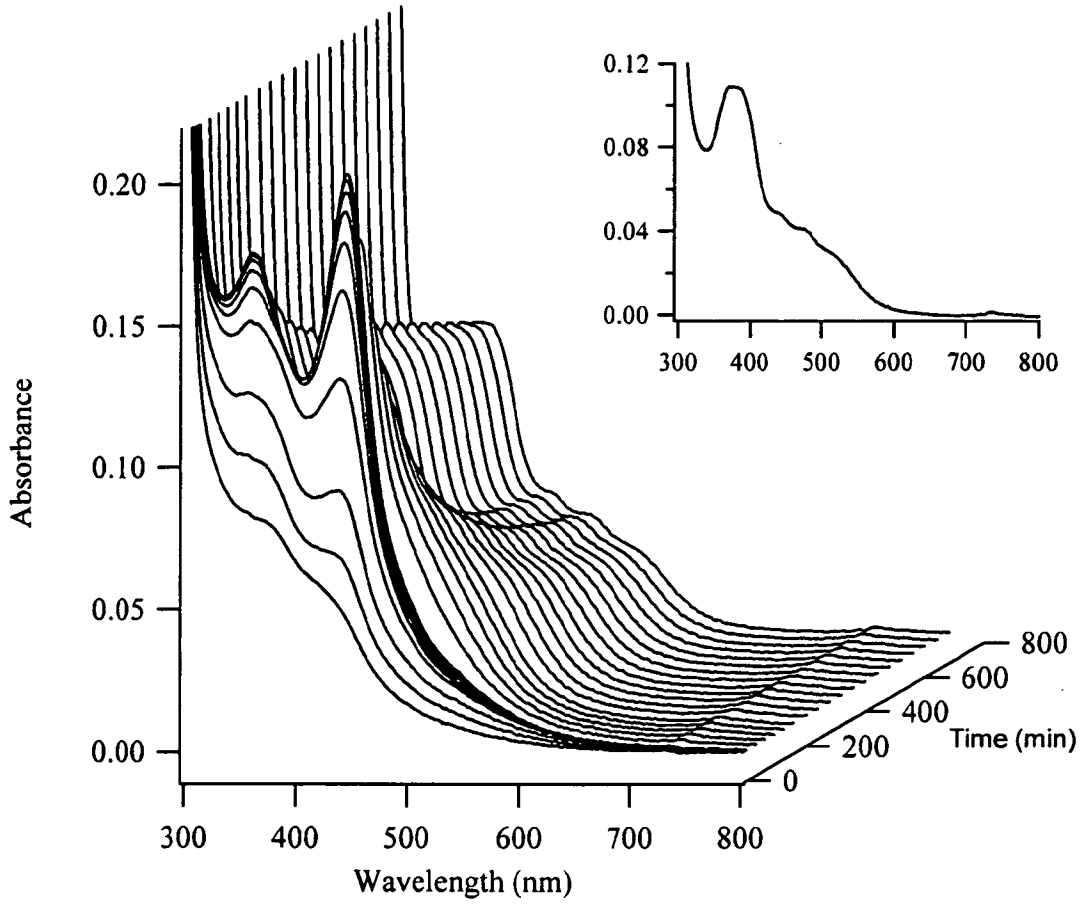

Fig 8. Absorption spectra associated with the DNA-bound silver nanoclusters using 1 Ag^+:10 bases. For these spectra, [oligonucleotide] = 10 μM, [Ag^+] = 12 μM, and [BH_4^-] = 12 μM. The first ten spectra were acquired every 2 mins after adding the BH_4^-, and the spectrum at 20 mins has λ_{max} = 440 and 357 nm. Subsequent spectra were acquired approximately every 40 mins. The inset spectrum shows the last spectrum in the series (704 mins) and a peak at 380 nm is observed. In addition, a broad emission band from 430 – 600 nm is observed.

[1] Link, S. & El-Sayed, M. A. Spectral properties and relaxation dynamics of surface plasmon electronic oscillations in gold and silver nanodots and nanorods. *J. Phys. Chem. B* **103**, 8410-8426 (1999).
[2] (a) Shipway, A. N. and Willner, I. Nanoparticles as structural and functional units in surface- confined architectures. *Chem. Commun.*, **20** 2035-2045 (2001). (b) Petit, C.; Taleb, A.; Pileni, M. P., Self-organization of magnetic nanosized cobalt particles. *Adv. Mater.*, **10**, 259-261 (1998).
[3] Crooks, R. M.; Lemon, B. I.; Sun, L.; Yeung, L. K.; Zhao, M. Q., Dendrimer-encapsulated metals and semiconductors: Synthesis, characterization, and applications. In *Dendrimers: Design, Dimension, Function*, 2001; Vol. 212, pp 81-135.
[4] Murray, C. B.; Kagan, C. R.; Bawendi, M. G., Synthesis and characterization of monodisperse nanocrystals and close-packed nanocrystal assemblies. *Ann. Rev. Mater. Sci.*, **30**, 545-610 (2000).
[5] Slocik, J. M. *et al.* Monoclonal antibody recognition of histidine-rich peptide encapsulated nanoclusters. *Nano Lett.* **2**, 169-173 (2002).
[6] (a) Braun, E.; Eichen, Y.; Sivan, U.; Ben-Yoseph, G., DNA-templated assembly and electrode attachment of a conducting silver wire. *Nature*, **391**, 775-778 (1998). (b) Niemeyer, C. M. Nanoparticles, proteins, and nucleic acids: Biotechnology meets materials science. *Angew. Chem.-Int. Edit.* **40**, 4128-4158 (2001).
[7] (a) Richter, J.; Seidel, R.; Kirsch, R.; Mertig, M.; Pompe, W.; Plaschke, J.; Schackert, H. K., Nanoscale palladium metallization of DNA. *Adv. Mater.*, **12**, 507-510 (2000). (b) Richter, J.; Mertig, M.; Pompe, W.; Monch, I.; Schackert, H. K., Construction of highly conductive nanowires on a DNA template. *Appl. Phys. Lett.*, **78**, 536-538 (2001). (c) Mertig, M.; Ciacchi, L. C.; Seidel, R.; Pompe, W.; De Vita, A., DNA as a selective metallization template. *Nano Lett.*, **2**, 841-844 (2002).
[8] Monson, C. F.; Woolley, A. T. DNA-templated construction of copper nanowires. *Nano Lett.* **3**, 359-363 (2003).
[9] (a) Peyser, L. A.; Vinson, A. E.; Bartko, A. P.; Dickson, R. M., Photoactivated fluorescence from individual silver nanoclusters. *Science*, **291**, 103-106 (2001). (b) Peyser, L. A.; Lee, T. H.; Dickson, R. M., Mechanism of Ag-n nanocluster photoproduction from silver oxide films. *J. Phys. Chem. B*, **106**, 7725-7728 (2002).
[10] Zheng, J.; Dickson, R. M., Individual water-soluble dendrimer-encapsulated silver nanodot fluorescence. *J. Amer. Chem. Soc.*, **124**, 13982-13983 (2002).
[11] Norden, B.; Matsuoka, Y.; Kurucsev, T., Nucleic Acid - Metal Interactions: V. The Effect of Silver(I) on the Structures of A- and B-Forms. *Biopolymers*, **25**, 1531-1545 (1986).
[12] Eichhorn, G. L. Complexes of Nucleosides and Nucleotides. In *Inorganic Biochemistry*; Eichhorn, G. L., Ed.; Elsevier: New York, 1973; Vol. 2, Chapter 33.
[13] Marzilli, L. G. Metal-Ion Interactions with Nucleic Acids and Nucleic Acid Derivatives. In Progress in Inorganic Chemistry; Lippard, S. J., Ed.; John Wiley and Sons: New York, 1977, Vol. 23, pp. 255-378.
[14] Luk, K. F. S.; Maki, A. H.; Hoover, R. J., Studies of Heavy Metal Binding with Polynucleotides using Optical Detection of Magnetic Resonance. Silver(I) Binding. *J. Amer. Chem. Soc.*, **97**, 1241-1242 (1975).
[15] Yamane, T.; Davidson, N., On the complexing of deoxyribonucleic acid by silver(I). *Biochim. Biophys. Acta*, **55**, 609-621 (1962).
[16] Dattagupta, N.; Crothers, D. M., Solution Stuctural Studies of the Ag(I)-DNA complex. *Nucleic Acids Research*, **9**, 2971-2985 (1981).
[17]Harbich, W.; Fedrigo, S.; Meyer, F.; Lindsay, D. M.; Lignieres, J.; Rivoal, J. C.; Kreisle, D., Deposition of Mass Selected Silver Clusters in Rare-Gas Matrices. *J. Chem. Phys.*, **93**, 8535-8543 (1990).
[18] Rodger, A.; Norden, B. *Circular Dichroism and Linear Dichroism* (Oxford, New York, 1997).
[19] Bonacic-Koutecky, V.; Pittner, J.; Boiron, M.; Fantucci, P., An accurate relativistic effective core potential for excited states of Ag atom: An application for studying the absorption spectra of Ag-n and Ag-n(+) clusters. *J. Chem. Phys.*, **110**, 3876-3886 (1999).
[20] Marchetti, A. P.; Muenter, A. A.; Baetzold, R. C.; McCleary, R. T., Formation and spectroscopic manifestation of silver clusters on silver bromide surfaces. *J. Phys. Chem. B*, **102**, 5287-5297 (1998).

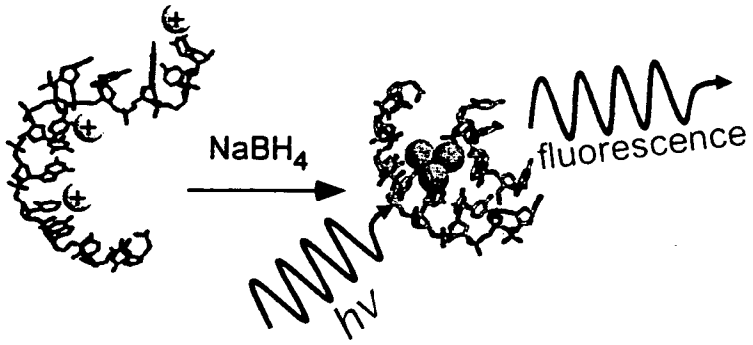
NaBH4
fluorescence
hv

A. Specific Aims

Understanding the inherent heterogeneity within living systems demands the development of new *in vivo* single molecule (SM) optical methods to follow protein dynamics without the veil of ensemble averaging.[1,2] Only through such high sensitivity SM methods can the promise of real-time characterization of dynamic cellular processes be fully realized. Although many fluorophores can be utilized in single molecule microscopy, continued advances are highly dependent on creating new fluorophores with greatly improved photophysical properties. Current fluorescent labels suffer from rapid photobleaching, low signal to background on the single molecule level, and often difficult synthetic attachment chemistries that can limit both *in vitro* and *in vivo* applications. Recently we have shown[3-5] that non-toxic dendrimer-encapsulated noble metal nanoclusters (<1-nm diameter) show extremely strong, robust, size-dependent single molecule fluorescence[6-9] and even single molecule Raman emission, but at much smaller sizes than either semiconductor quantum dots (3-10 nm diameters),[10,11] or more common Raman-enhancing metal particles (40-100 nm diameters).[12-14]

The bright fluorescence and Raman-enhancing abilities of noble metal nanoclusters enables us to create ultrasmall biolabels with two orders of magnitude stronger emission than any other known fluorescent label. Through a modular synthetic chemical approach, we will incorporate unique nanodot fluorescence and Raman signatures while simultaneously attaching and characterizing membrane transport and protein recognition units on the nanodot surface, thereby transforming them into specific, ultrabright *in vivo* single molecule fluorescence and Raman labels in background-free spectral windows. In addition, we will develop new strategies to create genetically encoded motifs that ultimately result in ultra-small, membrane transportable, targeted, genetically programmed biolabels with nearly ideal optical properties. Temporal and spectral gating will further enhance sensitivity to enable direct observation of single molecule dynamics with weak excitation and very low background, even in the presence of strong autofluorescence. The chemical schemes employed will create a modular, multi-functional array of nanodot probes ideally suited for targeted *in vivo* imaging of individual proteins. These metal nanocluster-based[4,15-20] modular, tunable, ultrabright, targeted, and biologically specific labels will singularly enable direct labeling and following of *in vivo* single protein dynamics with high temporal and spatial resolution.

Specific Aim I. Create modular single molecule fluorescence and Raman nanodot probes. We have developed Au and Ag nanocluster fluorescent and SM-Raman active species through biocompatible poly(amidoamine) dendrimer (PAMAM) encapsulation.[4,20] We will develop these strongly absorbing and emitting materials as modular single molecule fluorescence and Raman labels to penetrate membranes and bind specific proteins within the cytosol of living eukaryotic cells. Through targeted chemical derivitization including 'click' chemistry and thiourea linkages of both the outside and inside of PAMAM or PAMAM analogs, we will develop the modularity in the PAMAM scaffold necessary to incorporate functional groups for modular attachment of biochemical targeting and recognition motifs. We will also modify the PAMAM core to incorporate and characterize Raman active vibrations for unique narrow optical signatures.

Specific Aim II. Build and assay biological specificity. Dendrimer-encapsulated nanodots can already be employed as small, extremely bright biocompatible labels. To further expand the modularity of Ag and Au nanodot labels, we will develop bifunctionalized conjugates, which combine modifiers to increase cellular uptake and various affinity-tags to label proteins *in vivo*. The modifiers will be attached through the 'click'-chemistry detailed in Specific Aim I. Various membrane transport mechanisms will be assayed by measuring the kinetics of internalization as a function of various uptake signals. Membrane transport peptides and biochemical recognition/fusion protein binding units will be combined onto PAMAM dendrimers *via* an orthogonal bifunctionalization strategy. Nanodots created from these species will be compared against the uptake of monofunctionalized nanodots. Specific molecules targeting specific subcellular compartments will also be attached and examine their efficiency in directing nanodots to different pre-determined organelles. The single molecule and bulk optical properties of these functionalized nanodots will also be fully characterized for subsequent *in vivo* use in Aim III.

Specific Aim III. Intracellular single molecule labeling, specificities and protein dynamics. Further expending the versatility of our modular biolabels, short peptide sequences that specifically recognize functionalities on the dendrimer nanodot will be identified through solution-based library screening, a strategy that will create genetically encoded domains that 'capture' our ultrabright, membrane transportable nanodots. In addition, lock and key mechanisms (biotin-avidin) and catalytic covalent linkage (hAGT-BG) of nanodots to fusion proteins will first be characterized *in vitro*, followed by *in vivo* assays through both single molecule and bulk methods. The binding constants and labeling efficiencies will be probed both *in vitro* and *in vivo* and their influence on protein activity will be characterized by biochemical and biophysical methods. By utilizing a ligand-triggered protein trafficking system, progesterone receptor translocation, we will gate the flow of labeled protein into the nucleus to study the dynamics and assay its efficiency. New optical discrimination methods enabled by the unique nanodot optical properties will be employed to directly image individual proteins, even in the presence of strong autofluorescence.

Future extensions of the targeted specific labeling technologies developed through this exploratory center proposal.

Together, these studies provide a complete toolset for creating strongly fluorescent and Raman active noble metal nanoclusters with ~100 times stronger emission than the best available labels. The fast time response and extremely low photobleaching combined with the narrow temporal and spectral windows offer opportunities for measuring very fast and long time single protein dynamics within living systems, even in the presence of strong autofluorescence. The chemical functionalization to incorporate not only specific Raman signatures, but also modularity in membrane transport and fusion protein recognition and binding, offers a complete set of labeling tools that can be readily adapted to image various dynamic cellular processes. These studies will be broadened beyond the scope of this exploratory period to create chemically sensitive Raman sensors, infrared and near infrared emitters, energy transfer pairs, and dual function probes (as Au_{31} should be readily observable with electron microscopy). In the future, this modular approach will lead to an exponentially larger array of tools capable of rendering individual molecules and their dynamics in living cells readily observable to even the most inexperienced of researchers.

B. Background and Significance

*1. **Contrast generation in single molecule optical microscopy.*** Several key *in vitro* experiments ranging from RNA and protein folding to molecular motor motion have uniquely demonstrated the ability of single molecule microscopies to unravel the crucial steps leading to *in vitro* biological activity.[1-3,21-38] Unfortunately, the problems resulting from fluorescent labels become increasingly acute on the single molecule level and completely preclude studying *in vivo* dynamics. Although complementary in information content to ensemble studies, single molecule experiments present an extreme limit in which weak signals must be observed on essentially zero background.[39,40] By yielding time averages of many individual systems, single molecule studies enable bulk-obscured nanometer scale environmental interactions to be directly probed,[1,41-43] without the need of difficult external synchronization.[21,23-25,27,44] Unfortunately, current reliance on artificial fluorescent labeling of proteins of interest not only limits single molecule studies to *in vitro* observation, but also severely limits the timescales over which dynamics can be followed. Even for *in vitro* single molecule studies, excitation rates must be very high to yield biologically relevant information with reasonable time resolution (ms to seconds) and good signal to noise. Because the absorption cross-section (extinction coefficient, ε) of the best organic fluorophores is only $\sim 10^{-16}$ cm^2 ($\varepsilon \sim 10^5$ M^{-1}cm^{-1}) at room temperature,[38] high intensity laser excitation must be utilized for single molecule fluorescence studies. Additionally, organic molecules can only withstand $\sim 10^6$ excitation cycles before they photochemically decompose.[2,30,38] At 10^6 excitations/second (using $\sim$5kW/cm^2 excitation intensity and a typical collection/detection efficiency of 5%), this limits the time resolution to ~1 ms (with an idealized signal to noise ratio of ~7), and the average total time to follow an individual molecule before photobleaching to ~1 second. While this can be a large amount of data on very biologically relevant timescales, many of the excitation cycles end up being consumed by finding the molecules of interest before collecting data. Relying on the introduction of artificial labels to identify the particular protein or structure of interest, all fluorescence based methods suffer from two additional problems – photobleaching (loss of signal due to probe destruction) and autofluorescence (naturally occurring background fluorescence from native species within biological media). Such optical methods relying on high-intensity laser excitation of highly emissive and robust fluorophores require not only extremely efficient background rejection, but also the development of new nanomaterials with improved optical properties. Even with these problems, fluorescence microscopy remains the primary optical method with potential for single molecule and chemical sensitivity while imaging biological media. **Thus, advances in label properties will be crucial to the continued success of all single molecule optical studies in biological systems.**

*2. **Attachment chemistries.*** Most *in vitro* fluorescent labeling is performed through standard chemical coupling of either N-succinimidyl ester-conjugated dyes to free, solvent-exposed amines (often on lysine residues) or maleimide-conjugated dyes to thiols on either naturally occurring or genetically introduced solvent-exposed cysteines. These two coupling chemistries continue to be extremely useful in attaching small, highly fluorescent dyes to proteins of interest. Such fluorescent biomaterials are then adequate for *in vitro* single molecule studies, or they can be re-introduced into cells in high concentration either through microinjection or other membrane transport methods to perform bulk fluorescence studies of the protein of interest within whole cells. Because of photobleaching, low excitation rates, high *in vivo* background, often non-specific labeling, and difficult *in vivo* incorporation, studying dynamics of few copies of proteins within living systems requires the development of targetable, specific, membrane permeable, ultrabright and photostable probes such that they can specifically label proteins of interest inside cells and be easily observed with weak illumination for long times. Such illumination would enable preferential excitation of the fluorophores of interest relative to that of weak background signals. Unfortunately, as available dyes and specific attachment chemistries are limited, single molecule sensitivities are as of yet difficult to attain in such high background *in vivo* studies and are often difficult to observe even in lower background *in vitro* studies.

*3. **Improvements over standard fluorescent labels***

*3.a. **Water-soluble quantum dots as biolabels.*** Requiring similar attachment chemistry to that of organic fluorophores, water soluble II-VI quantum dots have recently been proposed and demonstrated as biological labels.[10,11,45] Materials such as CdSe with protective and stabilizing ZnS overcoatings have size dependent optical properties and can be synthesized with very narrow size distributions.[46-48] The strong absorption, spectral stability, and size-tunable narrow emission of these nanomaterials suggest exciting possibilities in biolabeling once further chemistry on the outer ZnS layer is performed to passivate, solubilize, and functionalize these materials.[10,11,49-58] While quite promising due to their bright and very narrow size-dependent emission, multiple problems with using CdSe as biological labels still exist. CdSe quantum dots are comparable to the size of proteins that they may label (3-10 nm in diameter), and they suffer from the same need to externally label proteins of interest and re-introduce the labeled proteins into cells. While offering reduced photobleaching, their absorptions are very broad, thereby precluding their use as energy transfer pairs. Fundamentally, these semiconductor quantum dots absorb very strongly ($\varepsilon \sim 10^7$ M^{-1}cm^{-1}, or ~100x that of a good organic fluorophore) with energy funneling down to the lone emissive bandgap level. Unfortunately, one must wait for a time corresponding to the quantum dot fluorescence lifetime (of ~10 ns) for emission to occur. This long radiative lifetime limits the total light out of quantum dots, and in fact, makes them only comparable in brightness to organic fluorophores (that have similar radiative lifetimes). The advantage is that they can produce the same number of photons/second as organic fluorophores with much weaker excitation. Consequently, these nanomaterials enable background reduction due to their strong absorptions relative to the organic fluorophores, but they do not increase signal intensity. Thus, while the strong oscillator strengths enable quantum dots to be easily observed with weak mercury lamp excitation, thereby avoiding much of the more weakly absorbing autofluorescent background, they are neither an ideal solution to *in vivo* nor *in vitro* single molecule studies.

*3.b. **Protein-derived biological labels.*** Ideally, one would want the smallest possible genetically programmed label to be expressed on the protein of interest. Such an ideal label would need to have sufficiently strong absorption and emission as well as outstanding photostability to enable long time single molecule observation with high time resolution, even in the presence of high background

fluorescence. Unfortunately, such a fluorescent probe does not yet exist. Composed solely of amino acids, green fluorescent protein (GFP)[2,59-64] is an excellent *in vivo* label, and has even been observed on the single molecule level in *in vitro* studies by many authors.[2,65-72] In one of the first such studies, we characterized GFP blinking and optical switching abilities as we used photons to shuttle the GFP chromophore between two different optically accessible states.[2] Unfortunately, while GFP can be specifically attached to the N or C terminus of any protein and expressed *in vivo* as a highly fluorescent label, problems, especially on the single molecule level, still remain. Emission only occurs once GFP has folded into its final conformation, a process that can take up to ~1 hour and, while examples of GFP labeling have been reported within all regions of different cells, sometimes GFP does not properly fold under a given set of conditions.[59,63] Additionally, when considering single molecule studies, its emission significantly overlaps with the autofluorescent background, but its emission intensity is only comparable to standard exogenous organic dyes, thereby making *in vivo* single molecule studies unrealistic. While largely insensitive to oxygen, it also typically bleaches after ~10^6 excitation cycles, similar to standard organic dyes.[2] DsRed[73-76] partially circumvents the issue of overlap with autofluorescent background, but while the red-shifted emission of DsRed relative to that of GFP could be an advantage, its comparable fluorescence intensity and tendency to form quadruplexes even at extremely low concentration limit its use as a biological label.[68,70,77,78]

3.c.Noble metal nanocluster fluorescence. Metals exhibit a particularly wide range of material behavior along the atom to bulk transition.[6,79,80] At sizes comparable to the Fermi wavelength of an electron (~0.5 nm), optical properties are significantly modified and discrete nanocluster energy levels become accessible.[79,80] Such metal nanoclusters, composed of only several tens of atoms exhibit molecule-like transitions, as the density of states is insufficient to merge the valence and conduction bands.[3,4,6,81,82] Recently, we utilized PAMAM G4-OH and G2-OH dendrimers (4th and 2nd generation OH terminated poly(amidoamine)s, Figures 1&4) to stabilize, and solubilize extremely small Ag and Au nanoclusters.[4,20,81,82] Conferred on Au and Ag nanodots only at the nanoscale, these size-dependent metal nanodots have strong oscillator strengths and very high fluorescence quantum yields in water (~50%), but at much smaller sizes than any other nanomaterial.[4,20,81,82] Similar to much larger semiconductor quantum dots, excitation is ~100x stronger than the best organic dyes and emission energy increases as nanocluster size shrinks. Most importantly, the discrete excitations and extremely short radiative lifetimes (~30 ps, Figure 2) coupled with the high fluorescence quantum yields enables these nanoclusters to emit nearly three orders of magnitude more photons/second than even semiconductor quantum dots. This singular advance opens possibilities of using noble metal nanodots as bright, photostable, and size-tunable biolabels (e.g. Figure 3). Additionally, the potential for harnessing the extremely strong pre-plasmonic electronic transitions of Au and Ag nanoclusters for Raman spectroscopy on the single molecule level not only suggest exciting applications in biolabeling with sub-nanometer Raman probes, but also eventually developing ratiometric Raman sensors for measuring intracellular concentrations and single molecule dynamics.[3,5] **With absorption strengths comparable to those of much larger quantum dots, these strongly absorbing, fluorescent, potentially Raman-enhancing (see Preliminary Results section), and photostable noble metal nanodots will be employed as high-brightness, targeted *in vivo* single molecule biolabels.**

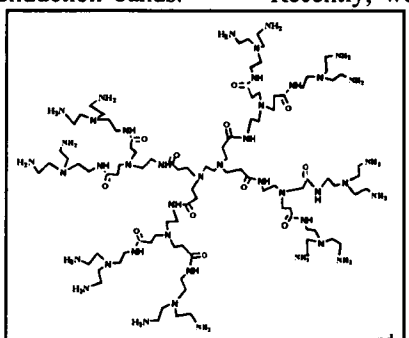

Figure 1. Structure of 2nd generation NH_2-terminated poly-(amidoamine) dendrimer, G2-NH_2.

4. Raman microscopies and single molecule SERS

Surface enhanced Raman spectroscopy (SERS). In the 1970s, it was discovered that Raman (vibrational) signals are greatly enhanced (~10^6-fold) near roughened metal surfaces.[83-87] Originally postulated to arise from the strong electromagnetic field enhancements near silver surfaces, observed surface enhancements were often larger than could be ascribed to this effect alone. In 1984, Hildebrandt and Stockburger reported detection of ~10^{-9} M rhodamine 6G with SERS[88] – a result requiring an enhancement of ~15 orders of magnitude. This observation portended the recent reports of single molecule SERS (SM-SERS) that require a similar unexplainably large enhancement usually ascribed to nebulous electromagnetic and resonance Raman enhancements in the near field of silver nanoparticles.[12-14,89,90]

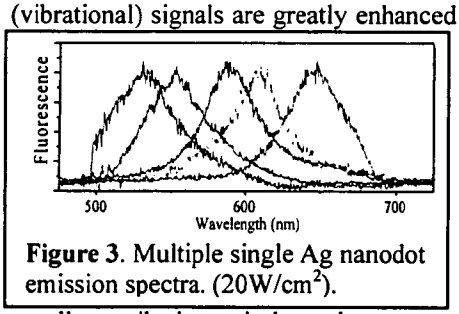

Figure 3. Multiple single Ag nanodot emission spectra. (20W/cm^2).

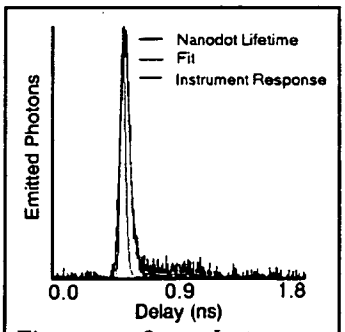

Figure 2. Instrument response (red) and 23-psec single exponential fit (green) to individual Ag nanodot lifetime decay (grey).

SERS provides important vibrational information on molecules within complex chemical systems. Thus, while only certain modes are enhanced, surface enhanced Raman spectroscopy (SERS) is the only tool that can truly combine chemical information with single molecule sensitivity. Although Raman is a weak effect, it is actually stronger on the single molecule level than is fluorescence.[12-14,88] This results from the instantaneous nature of the Raman process, thereby increasing total emission rates and preventing photobleaching. Currently, SERS is impractical for labeling due to the need to amplify Raman signals with very large (≥ 50-nm diameter) highly absorbing and scattering Au or Ag nanoparticles as Raman contrast agents for molecules very close to the metallic surface.[83-88,91] As only a subset of particles give this enhanced response and the full enhancement cannot be explained with theory, the chemical and physical interactions giving rise to the enhancement and its associated fluorescent background remain elusive. Unfortunately, while Raman signals do not bleach, the large Ag and Au Raman contrast enhancing nanoparticles are incompatible with *in vivo* biological imaging.

Crucial to most SM-SERS arguments is the existence of "hot spots" or binding sites exhibiting unique enhancements. In fact, silver colloids specifically prepared without surface-bound clusters do not yield enhancements sufficient for single molecule sensitivity.[14,92,93] Classically, Raman spectroscopy occurs through an external electric field (e.g. a laser) polarizing the molecule, thereby inducing a dipole moment at the excitation frequency (Rayleigh scattering), and at the sum and difference frequencies between molecular vibrations and the excitation source to yield the Raman signal. The classical description relates the induced dipole, μ, to the applied electric field, E, through the polarizability tensor, α. Quantum mechanically, of course, the Raman transition moment (i.e. polarizability matrix elements) is given by the Kramers-Heisenberg-Dirac formula (equation 1).

In accord with Equation 1, the laser polarizes the molecule to connect the initial, $|i\rangle$, and final, $|f\rangle$, vibrational levels by mixing each with all available electronic states, $|m\rangle$. The resulting inelastic Raman scattering from the intermediate to the final state deposits vibrational energy in the molecule. As the energy difference between the incident laser (E_{laser}) and any of the strongly allowed electronic transitions between states $|i\rangle$ and $|m\rangle$ (E_{mi}) becomes small, strongly enhanced Raman transitions occur with a homogeneous linewidth, Γ. This resonance Raman process occurs through the resonant driving of an electron between dipole-connected electronic states. Consequently, the extremely strong absorption of Ag nanoclusters ($\sigma \sim 10^{-14}$ cm^2) directly contributes to the very strong Raman signals on Ag nanoparticles.

$$\langle f|\alpha_{Raman}|i\rangle = \langle f|\sum_m \frac{\mu_{fm}|m\rangle\langle m|\mu_{mi}}{E_{im} - E_{laser} - i\Gamma}|i\rangle \quad (1)$$

CARS (Coherent Absorption Raman Spectroscopy) imaging. Due to its reliance on the presence of large nanoparticles for high Raman contrast, Raman imaging has yet to approach the single molecule level in anything even approximating a real biological system. Xie and co-workers,[94-99] however, have developed a novel zero-background nonlinear optical microscopy, CARS, to image live cells with chemically relevant information. By probing the C-H stretch frequency, for example, they were able to differentiate lipids from cytoplasm and begin to image different organelle structures with good optical resolution and sensitivity. While promising, this exciting technique depends nonlinearly on the number of vibrational modes of a given frequency in any molecule. Therefore, this method has yet to reach the sensitivity limits necessary to image and assay the dynamics of individual copies of a given protein. Clearly for linear and nonlinear Raman imaging of living systems to reach the single molecule level, nanoscale Raman contrast agents must be created and specifically bound to proteins.

5. Biological scaffolds for materials science.

Dendrimers. Having found many uses in recent years, dendrimers are highly symmetric branched polymers that can be created with well-defined and pre-programmed shapes, molecular weights, chemical properties, and perfect polydispersities.[100-105] Dendrimers are defined by their generations or the number of shells of a given chemical composition counted outward from the center.[103] Although hyperbranched or starburst dendrimeric structures have been created from many different monomeric units,[101,106] one of the most intriguing is the biocompatible poly(amidoamine), or PAMAM,[104,107,108] portrayed in Figure 1. This water-soluble dendrimer has a peptide-like amide-based backbone and has found great utility in applications ranging from templates for nanoparticle synthesis (Figure 4)[109-113] to controllable release scaffolds for drug and gene delivery.[16,104,114-118] In fact, PAMAM has not only shown great proficiency in readily penetrating tissues[119-121] and cell membranes,[122-124] but its biodegradability further bolsters its potential for intracellular cargo delivery.[115,125-127] Such well-controlled dendritic structures are easily made to have well-defined interiors and exteriors for differential functionalization and tailoring to a wide variety of applications.[101,111,114,123,128]

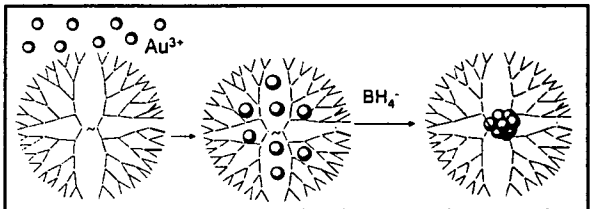

Figure 4. Au nanodot production. Fourth generation PAMAM dendrimers interact with Au^{3+} ions, which are subsequently photoreduced with UV light or chemical reductants to create metal nanoclusters inside the dendrimer core.

While single molecule methods have been effective in "peeling back" the ensemble average to examine environmental and mechanistic heterogeneity, current techniques remain fundamentally limited by the poor optical properties, bioincompatibility of available fluorescent labels and the narrow timescale window accessible to single molecule observation. Nanotechnology has yet to ameliorate these problems. New single molecule probes must therefore be created with greatly improved photostability, much stronger absorption and emission under weak illumination, facile synthesis and conjugation to proteins, and tunable emission color. Ideally, such ultrabright labels should also contain chemically specific information and be genetically programmable such that proteins under study can be directly labeled intracellularly, without first being overexpressed, purified, labeled, and subsequently reintroduced into cells. The combination of extremely strong Ag and Au nanocluster fluorescence and Raman enhancing capabilities (see Preliminary Results) combined with bioinspired materials such as PAMAM dendrimers have enabled us to create fluorescent materials that meet or exceed most of these stringent requirements. Further employing chemical and biological diversity in conjunction with nanocluster optical properties will enable direct, ultrasensitive labeling of proteins using Raman tags to follow single protein dynamics within living systems. The materials and methods developed in this proposal will provide a set of tools that are generally applicable to *in vivo* single molecule studies. Most importantly, the proposed ultra-bright probes will provide sufficient signal to be readily observed in nearly any environment with unprecedented sensitivity.

C. Preliminary Results relevant to Specific Aims.

Creation and characterization of strongly emitting Au and Ag nanodots. We demonstrated the facile synthesis of Au and Ag-containing dendrimer nanodots through sequestering metal ions into PAMAM dendrimers[4,109,129,130] followed by reduction using either photoactivation with weak UV light or standard reducing agents, maintaining neutral pH. The reduced metal atoms aggregate within the

dendrimers to form small nanodots (dendrimer-encapsulated nanoclusters) and large nanoparticles, which are readily removed by centrifugation.[109] Simply by adjusting the initial concentration ratios, we can tune Ag and Au nanodots excitation and emission throughout the visible and near-IR region (Figures 3,5 & 6). Such nanodot solutions exhibit no characteristic surface plasmon absorptions, and the mass spectra (enabled by the precise dendrimer molecular weight, Figure 5) clearly reveal well-defined nanoclusters within the PAMAM host. The extremely strong electronic transitions and high fluorescence quantum yields of these small metal nanoclusters (≤1-nm in size for both Au (5-31 atoms) and Ag (2-8 atoms)) make them as strongly absorbing as much larger CdSe quantum dots, but more than 100x brighter due to their much faster radiative lifetime (Figure 2).[81,82] These dendrimer-metal based nanodots can be dried and re-dissolved without changing the optical properties. The symmetry of absorption and emission (Figure 6) clearly indicates that emission is more molecular in nature than from quantum confined bands of semiconductor quantum dots which do not exhibit discrete absorptions. Amazingly, fluorescence quantum yields for G4-OH and G2-OH encapsulated gold nanodots range from 70% for the UV emitting species (Au_5) to ~20% for the near IR species (Au_{31}) – 2-3 orders of magnitude higher than observed for any other Au species and comparable to the best available fluorophores. The extinction coefficient increases significantly for Au as one moves farther out in the near IR and the lifetime shortens to less than 1 ns. Ag nanodots, on the other hand all have extremely short lifetimes (~30ps, Fig. 2) with >30% quantum yields due to excitation of electrons in the highly polarizable pre-plasmon transition. This short lifetime and high quantum yield mean that many more excitations/second can occur, thereby giving orders of magnitude higher signal than even similarly absorbing, but much longer lived (~10 ns) and more rapidly photobleaching semiconductor quantum dots.

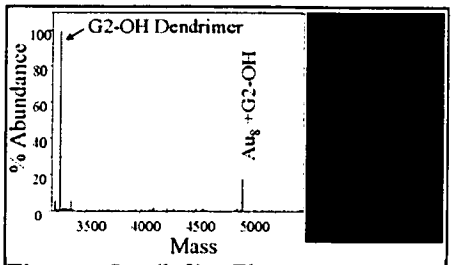

Figure 5. (left) Electrospray mass spectrum of blue-emitting G2-OH PAMAM encapsulated Au nanoclusters. (right) Emission from G2-OH encapsulated gold nanodots under long-wave UV lamp irradiation (~366 nm).

The important concept here is that as one moves to excitation energies lower than the characteristic plasmon absorptions (~390 nm for Ag, ~520 nm for Au), transition strengths become extremely strong due to collective oscillation of electrons. The plasmon in such nanoscale metal species is more discrete in nature and leads to the unprecedented strong emission. As shown in Figures 7 and 8, these species are readily observable on the single molecule level with excitation strengths up to 100 times stronger than the best organic dyes. **It is precisely these extremely strong optical transitions that, according to Equation (1), can lead to very high polarizabilities and to single molecule Raman (SM-Raman) signals from the scaffold encapsulating the sub-nm noble metal nanocluster.** Thus, we will utilize both the extremely strong SM fluorescence and the SM-Raman for *in vivo* biolabeling.

Ag nanoclusters as scaffold-specific single molecule Raman contrast enhancement agents. By exciting slightly longer wavelength than both the optical transition and the surface plasmon excitation, we have observed strong, blinking, SM-Raman spectra from our dendrimer and peptide encapsulated individual nanodots. With Ag nanoclusters as the contrast agents, these highly scaffold specific Raman signals are readily observed under 514-nm excitation (Figure 7), while Au nanodots need to be excited in the near IR to yield SM-Raman transitions, both in accord with SM-SERS signals observed from dyes adsorbed on surfaces of much larger Ag and Au nanoparticles. These observations demonstrate that only the nanocluster (not the large nanoparticle) interacting with the organic scaffold is necessary to produce Raman signals on the single molecule level and yield the observed wavelength dependence on excitation. Consequently, SM-Raman does not need large nanoparticles to be observed on the single molecule level – the few-atom-sized, strongly absorbing, pre-plasmonic Ag or Au nanoclusters are sufficient to yield strong SM-Raman signals with 100x larger cross sections than the best organic fluorophores and emission rates >100x higher than even much larger semiconductor quantum dots due to the extremely fast and efficient radiative decay. While individual molecules have very different spectra, each is specific to the surrounding scaffold. While both the fluorescence and Raman enhancing properties of these noble metal nanoclusters will be developed and utilized in this proposal, **the Raman effect provides unambiguous scaffold-specific information on the single molecule level.** Additionally, by only looking within a very narrow spectral window corresponding to the vibrational frequency shift from the laser energy, the strong, very narrow (vibrational) linewidth further reduces background but maintains very strong single molecule signals. Whether individual features are probed with Raman spectroscopy or the spectra of many individual features are summed (Figure 8), clear differences are observed that are

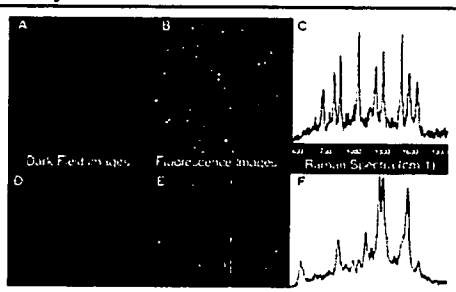

Figure 7. (A-C) Peptide darkfield (A) and emission (B) images of the same field of view. Vertical lines correspond to the monochrometer slits used to take the spectrum in (C). The sharp lines are Raman transitions characteristic of the peptide scaffold. Only features not observed in the darkfield images were studied – proving that SM-Raman arises from nanodots smaller than 2 nm (the lower limit of observability in darkfield microscopy). (D-E) The corresponding darkfield image, emission image, and SM-Raman spectrum of the PAMAM scaffold enhanced by the Ag nanocluster it surrounds.

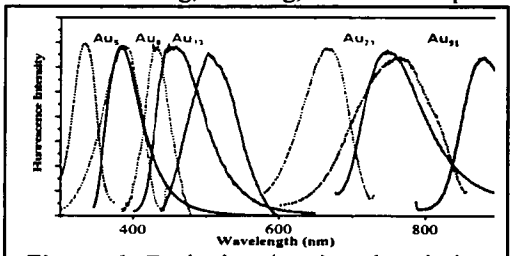

Figure 6. Excitation (-----) and emission (—) spectra of different strongly fluorescent Au nanodot solutions. Identical colors are used for excitation/emission spectra of the same species.

characteristic of the nanodot-encapsulating scaffold. By exciting longer than the surface plasmon frequency of the bulk metal, one can clearly observe the enhanced Raman on the single molecule level. It is this observation that enables SM-Raman as an *in vivo* label with chemical information. Because of the narrow linewidths, an order of magnitude increase in sensitivity is possible solely due to background reduction of the broad autofluorescence by looking in a narrow spectral window that contains only the Raman emission.

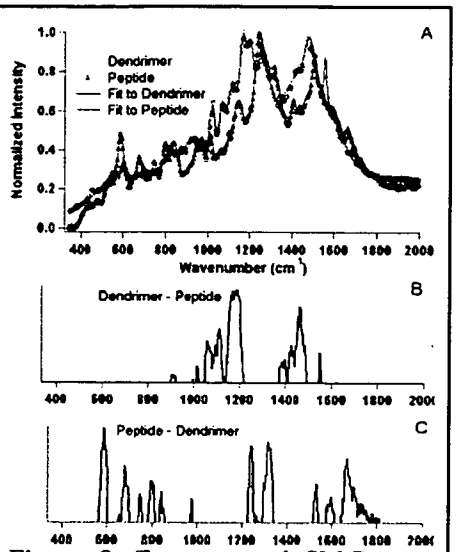

Figure 8. Top: summed SM-Raman spectra (50 molecules each) of peptide (red) and dendrimer (blue). Bottom: difference spectrum indicating clear differences in Raman spectra as a function of nanodot scaffold

Peptide encapsulation of metal nanodots. We have demonstrated that a short 9-amino acid peptide can stabilize Ag_n nanocluster emission (Figure 7). This short peptide (AHHAHHAAD) was recently reported to interact with large metal and semiconductor nanoparticles upon reduction.[131,132] Using our gentle photoactivation procedures,[4] we have produced very highly emissive peptide-encapsulated nanodots. As reported above, not only do these peptide-encapsulated nanodots fluoresce with very short lifetimes and high quantum yields, but they also have strong SM-Raman signals with narrow features characteristic of the peptide scaffold.

Our gold and silver nanodots are very stable in both solution (even at high salt concentrations) and films and are readily observed on the single molecule level with chemically tunable emission properties, ultrabright fluorescent and scaffold-specific SM-Raman emission and reduced blinking (Figure 9). It is precisely the properties conferred upon nanoscale gold and silver when approaching the atomic level that we will exploit as in vivo single molecule biolabels. **With synthetic control of nanodot attachment and Raman enhanced vibrational modes, such simple nanomaterials will become an entire new class of quantum dots with great potential as biological labels. Due to their discrete absorptions, small size, and size tunability, they promise to become effective nanoscale materials for high sensitivity *in vivo* single molecule imaging. The biocompatibility and nobility of gold and silver, combined with the exciting optical properties conferred on the nanoscale makes these strongly fluorescent and Raman-enhancing dots attractive new nanomaterials for studying individual biological systems and their dynamics on biologically relevant length scales within living cells.**

Summary. We have produced extremely small, highly emissive (both fluorescence and Raman) and very photostable, water-soluble Au and Ag nanodots consisting of only a few to a few tens of atoms encapsulated by biocompatible PAMAM dendrimers. The extremely advantageous optical properties have already yielded incredibly photostable and strongly absorbing and emitting species with size-dependent emission throughout the visible region. **We have assembled an outstanding team of investigators with expertise in single molecule microscopies (Dickson),[2-5,28,31,133-138] dendrimer synthesis and characterization (Weck), 'click' chemistry (Weck and Bunz), cellular uptake, sensing, and whole cell imaging (Fahrni), fusion protein expression and nuclear targeting in eukaryotic cells (Doyle), and library screening, bacterial expression, and protein biochemistry (Tzeng) to create and characterize even more powerful labeling methods specifically for *in vivo* single nanodot Raman and fluorescence experiments. The synergistic overlap of expertise also provides outstanding opportunities for discussion and cross fertilization of ideas within this group. The specific, multicolored labels developed through this exploratory center will enable unprecedented optical and chemical sensitivity necessary to perform *in vivo* single molecule experiments on any protein of interest with greatly enhanced signals and experimental simplicity. New ultrahigh brightness probe developments of this type are crucial to the general applicability and utility of single molecule methods in unraveling the complexities of biological systems.**

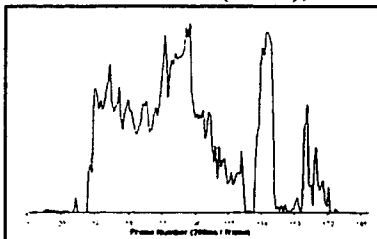

Figure 9. Blinking of Raman emission from PAMAM encapsulated Ag nanodot indicating single molecule Raman signals arising from the nanocluster-scaffold interaction.

D. Research Design and Methods.

We propose a coherent set of experiments and goals to produce and characterize modular, robust, bright, biological labels that are simultaneously very small, biocompatible, suitable for specific *in vitro* and *in vivo* labeling and easily observed on the single molecule level. The brightness and ease of synthesis will yield a 'toolbox' of biological labels that will enable researchers to easily perform single molecule dynamics studies in living biological systems. While our fluorescent nanodots are already extremely bright, SM-Raman spectroscopy is unique in its potential to provide chemical information within living systems. Our observation that Ag and Au nanoclusters act as local Raman contrast agents with single molecule sensitivity offers future applications in true chemical sensing on the single molecule level within cells. The methods developed through the proposed studies will greatly extend the applicability of single molecule techniques to an ever-increasing range of biological applications. As a result, through creating the proper biocompatible scaffold enhousing the nanodots, we will develop the technology for understanding and utilizing these ultrabright noble metal nanodots as versatile, targeted, *in vivo* single molecule fluorescence and Raman biolabels in background-free spectral windows.

Specific Aim I. Create modular single molecule fluorescence Raman nanodot probes.

Rationale. Size-tunable noble metal nanoclusters are attractive candidates for making the smallest possible labels with oscillator strengths suitable for *in vivo* single molecule imaging. Our overall goal is to develop strongly emissive Au and Ag-containing PAMAM dendrimers as single molecule fluorescence and Raman labels that will penetrate membranes, bind specific proteins, and be targeted to

specific regions within living eukaryotic cells. Through chemical derivatization to incorporate both specific biochemical recognition units and background-free vibrational modes into the dendrimeric scaffold, we will employ our sub-nm SM-Raman enhancing noble metal nanoclusters to create unique,[4,15-19] modular, tunable, ultrabright, targeted, and biologically specific labels for studying *in vivo* single protein dynamics. Thus, our first specific aim is to chemically derivatize both the inside and outside of the dendrimer scaffold to incorporate unique Raman active vibrations and create modularity in cellular targeting and protein labeling specificity, respectively. These two complementary paths will create modular PAMAM-encapsulated nanodots such that in subsequent Aims, any protein can be targeted through specific and direct labeling within the cytoplasm without the need of purification, external labeling, and re-introducing the labeled protein into the cell. Furthermore, this Aim will develop the modular single molecule labels and assay their single molecule optical properties and will introduce a general and modular attachment strategy.

Experimental approach.

I.A. Dendrimer design and synthesis. The dendridic scaffold of choice must meet a variety of requirements including 1) biocompatibility, 2) ease of functionalization in the core and on the surface, and 3) incorporation of the nanocluster inside the dendrimer. PAMAM dendrimers fulfill the first and third requirements.[104,114,139-144] Readily transported across cell membranes, the basic PAMAM dendrimers are commercially available and have been used extensively for gene and drug delivery as well as for nanoparticle encapsulation.[105,114,126,141,143,145-164] Furthermore, PAMAM dendrimers show no significant cytotoxicity up to generation six.[105,162-164] Based on our demonstrated ability to produce strongly fluorescent and Raman active noble metal nanoclusters less than 1-nm in diameter within biocompatible PAMAM, we suggest that PAMAM dendrimers are the ideal scaffold for *in vivo* noble metal nanodot biolabeling. Therefore, we will concentrate our studies initially on PAMAM-based dendrimers.

1. Basic dendrimer design and multifunctionalization considerations. Dendrimers contain three topologically different regions: the core, the branches, and the surface.[101,165-167] For our proposed studies, we require a) fluorescent nanocluster binding and unique Raman labels in the core and b) the possibility for specific multifunctionalization of the surface. In particular the latter requires the design of a dendrimer that can be functionalized with at least two different compounds in a well-defined and orthogonal fashion, *i.e.* without interference of one functional group during the functionalization of a second one. To develop such a dendrimer multifunctionalization strategy is nontrivial and a number of potential methodologies have been postulated and partially carried out (Figure 10).[101,167] The first strategy relies on dendrimer creation from differently surface-functionalized dendrons (Figure 10B) while the second strategy achieves random bifunctionalization of dendrimers by the stoichiometric control of reactants added to the dendrimer in either a step-wise or one-pot fashion (Figure 10C). The third strategy is based on the use of multifunctionalized monomers or building blocks (to be achieved through protection and deprotection steps) to gain access to multifunctionalized dendritic systems (Figure 10D).[164,168-172] Finally, it is also imaginable to combine the first and the third strategies to yield multifunctionalized dendrimers with very low percentage of one functionality (for example a dendrimer containing a single second functionality can be fabricated using a two-dendron dendrimer with a single functional group on one of the two dendrons). We propose to use all strategies in our studies and will evaluate each during the course of researching the most promising route(s).

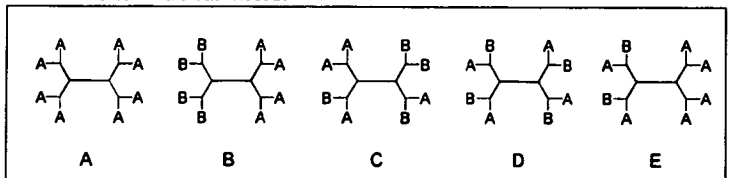

Figure 10. Multifunctionalization startegies for dendrimers. a) single-functionalized dendrimer, b) combination of different functionalized dendrons, c) Random difunctionalization, d) use of multifunctionalized monomers, and e) combination of strategies b and d.

2. Incorporation of SM-Raman tags: dendrimer core design and synthesis. As described above, PAMAM-encapsulated Ag and Au nanoclusters are highly emissive and offer exciting opportunities as *in vivo* single molecule biolabels.[4,109,173-181] They also produce strong, characteristic SM-Raman signals characteristic of the scaffold. As described in the preliminary results, to access nearly background-free spectral windows, functional groups as Raman labels will be incorporated into the dendrimer core. While the single nanocluster fluorescence is already brighter than that from other labels, Raman offers four key advantages over fluorescence: 1) extremely high emission rates due to even shorter lifetimes, 2) no photobleaching, 3) constant shift from the laser frequency even if exciting in the near IR, and 4) narrow emission to greatly reduce noise by limiting the spectral bandwidth. A variety of functional groups including carbon-deuterium (C-D) and triple bonds (C≡N, C≡C, C≡O) have vibrational frequencies outside the fingerprint and hydrogen stretching regions in the nearly background-free 1900~2300 cm^{-1} spectral region. If the proper excitation wavelength is chosen and especially if time-gated detection is used, SM-Raman offers nearly background –free imaging even in biological media. For ease of synthesis, we will focus initially on carbon-carbon triple bonds and deuterium labeled dendritic cores. Figure 11 outlines the proposed dendrimer cores.

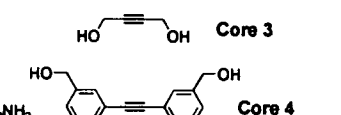

Figure 11. Proposed dendrimer cores.

Cores 1 and 2 contain deuterium instead of hydrogen on key carbons and are based on the original PAMAM core. Both cores are either commercially available (**Core 1**) or can be synthesized using standard PAMAM creation conditions: exhaustive Michael addition of amino groups with methyl acrylate followed by amidation of the resulting ester with ethylenediamine (**Core 2**).[104,167,182] It is important to note that this strategy allows us to place a deuterium label in any dendrimer generation we desire by using ethylene-d_4-diamine instead of ethylenediamine. Therefore, we propose to synthesize a library of PAMAM dendrimers of generation 1-5 *via* the divergent dendrimer synthesis approach with deuterium labels in each generation. This library will allow us to study and determine the optimal location and concentration of the Raman label in the dendrimer through single molecule Raman and fluorescence microscopy.

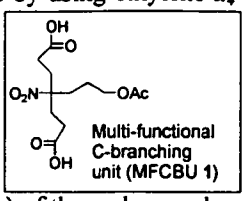

Cores 3-6 contain one or more carbon-carbon triple bond. These compounds are either commercially available (**Core 3**) or can be synthesized in one or two steps using standard palladium coupling chemistry (**Cores 4-6**). These cores are designed to a) increase systematically the amount (and ultimately the concentration) of the carbon-carbon triple bonds in the core to determine the optimal C≡C triple bond concentration and b) to study the effect of the number of dendrons (for example, **Core 3** has one acetylene unit and two alcohols which allow for two dendron-functionalization. In contrast, **Core 4** has also only one acetylene unit but four alcohols) on the proposed application. It is important to note that these cores can be used for either convergent (pre-synthesized dendrons assembled with the core molecule in the last step) or divergent (starting from the dendrimer core and building the dendrimer outwards) PAMAM syntheses.[167]

3. Dendron and basic dendrimer design and synthesis. PAMAM dendrimers can be synthesized easily *via* convergent or divergent methodologies and with amine, alcohol, ester, or acid functionalities on the surface.[104,105,142,162-164,167,171,172,182-184] In particular the convergent approach allows for the synthesis of multifunctionalized dendrimers using different dendrons. The most common PAMAM synthesis follows the divergent synthetic strategy outlined above in the core section by exhaustive Michael addition of amino groups with methyl acrylate followed by amidation of the resulting ester with ethylenediamine and extensive HPLC purification.[104,167,182] Using **Cores 1** and **2**, we will use this approach to synthesize dendrimers of generations 1-5. Due to the nature of the divergent methodology, these dendrimers will contain only amine functionalities on the surface, *i.e.* they are monofunctionalized, and will be functionalized as outlined in Figure 10, strategy C (**Dendrimers 1**). Furthermore, using literature procedures, we will synthesize a variety of dendrons based on the Michael-addition/amidation approach (**Dendrons 1**) for use in the convergent dendrimer methodology. Based on a recent report by Newkome and coworkers, we propose to synthesize bifunctionalized dendrons using the 1→2+1 C-branching monomer (MFCBU **1**).[171] Newkome demonstrated the synthesis of monofunctionalized second-generation PAMAM-analog dendrons with a single second functional group on the surface, *i.e.* all but one functional groups on the surface were either esters or acids resulting in a bifunctionalized dendrimer with a **SINGLE** second functionality on the surface. The lone surface alcohol group allows for subsequent specific mono-functional attachment of a single moiety onto the dendrimer surface. Using complementary chemistry and MFCBU **1** we will synthesize dendrons of generation 1-5 with well-defined multifunctional surfaces (**Dendrons 2**). We will also synthesize the non-MFCBU **1** containing complementary generations 1-5 dendrons, *i.e.* dendrons with a purely acid or ester containing surface (**Dendrons 3**). Furthermore, in analogy to the methodology described by Newkome, MFCBU **2** containing two alcohol groups and a single ester or acid group will be designed and synthesized using standard chemistry. Using protection and deprotection steps, generation 1-5 dendrons with variable concentrations of MFCBU **2** will be synthesized (**Dendrons 4**) resulting in dendrons with mainly alcohol functionalities and one or more (based on the design and synthesis) acid functionality. Furthermore, the non-MFCBU **2**, *i.e.* non-acid containing dendron-analogs to **Dendrons 4** will be synthesized yielding **Dendrons 5**. These five different dendrons will give us a) a tool box of dendrons with different surface functionalities and different degrees of surface multifunctionalization and b) the opportunity to design and synthesize dendrimers with well-defined functional groups, thereby allowing a modular approach toward dendrimer synthesis.

The composite dendrimers with Raman tags and pre-programmed surface functionalities will be synthesized using standard chemistry by reacting the dendrons with the dendrimer cores outlined above. It is important to note that in some cases an alkyl spacer with a terminal acid functionality will be introduced onto the core molecules thereby changing the functional group from an alcohol to an acid allowing for standardized amide formations between the cores and the terminal amines of the first generation of the dendrons. As outlined above, the proposed core molecules will give us the opportunity to vary the number of dendrons per dendrimer from two to six and ultimately control the extent of multifunctionalization on the surface of the desired and designed dendrimer. Again, through variations of the different dendrons used, we will be able to design and synthesize dendrimers that are mostly amine, alcohol, or acid functionalized, each containing a controlled number (one or more) of acid or alcohol functionalities. Furthermore, through dendron variations, we can synthesize dendrimers with a mixture of alcohols and acids each functionality class located on a single side of the globular dendrimer. For example, a 50% alcohol and 50% acid dendrimer could be a two-dendron dendrimer based on one dendron from **Dendron 5** and one from **Dendron 3** or a 33% alcohol and 67% acid dendrimer would be based on a three-dendron dendrimer based on one dendron from **Dendron 5** and two from **Dendrons 3**. In summary, this modular dendron/core convergent synthesis approach will allow for the controlled multifunctionalization of dendrimer surfaces while simultaneously incorporating Raman tags as acetylene or C-D bonds at controlled locations throughout the core and branches.

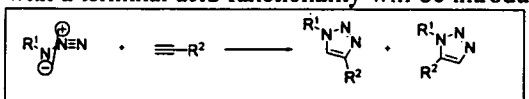

Figure 12. General scheme of 'click' chemistry

4. Incorporation of modularity in biospecificity: Dendrimer surface functionalization. To incorporate biospecific recognition units **AND** Raman labels **AND/OR** peptide sequences for peptide mediated protein delivery into cells (Aim II), orthogonal multifunctionalization schemes need to be developed. To minimize different surface chemistries, a modular surface functionalization scheme is desirable. The requirements for such a functionalization scheme are that the chemical transformations are fast and

quantitative, can be carried out under mild reaction conditions, can be generalized to a wide variety of potential functional groups, and are orthogonal to each other. In most cases, PAMAM dendrimers have been functionalized using amide or ester formations or through thiourea linkages.[101,105,141,142,162-164,167,171,172,183] Unfortunately, these transformations are **NOT** orthogonal to each other. We propose to introduce and use 1,3-dipolar cyclo-additions or 'click' chemistry as the second orthogonal transformation to multifunctionalize dendrimer surfaces.[185-188] 'Click' chemistry has been used in polymer systems but no example of 'click' chemistry in dendrimers has been reported. Furthermore, 'click' chemistry between an azide and an acteylene unit (it can be viewed as a 1-3 dipolar cycloaddition as outlined in Figure 12), is known to proceed quantitatively in water under very mild reaction conditions, and is tolerant to a wide variety of functional groups including amines, acids, and alcohols.[185-188] The only functional groups intolerant with 'click' chemistry are triple bonds and phosphines. The dendrimers are designed to NOT contain any phophines and no triple bonds on the surface of the dendrimers. It is important to note that the acteylene units in the core of the dendrimers are inaccessable to functionalized dendrimer surfaces due to the globular shape of the dendrimers and steric repulsions. Therefore, 'click' chemistry is orthogonal to all functionalization on the dendrimer surface and is the second chemical transformation of choice.

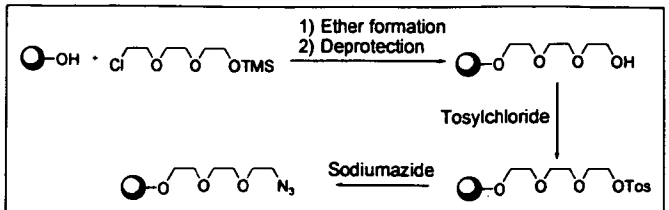

Figure 13. Proposed azide formation on dendrimers.

Azides are one of the two essential parts of 'click' chemistry and are stable to functional groups and most reaction conditions.[185] Azides, therefore, are the functional groups of choice for the 'click' chemistry on the dendrimer surface. As described above, we are able to create dendrimers with a wide variety and controllable density of surface functional groups. We propose to use the terminal alcohol moieties of the dendrimer surface to be the 'click' chemistry anchoring unit. Transformation of the alcohols into azides will be carried out in a three-step synthetic sequence as outlined in Figure 13. The resulting dendrimers will have either protected amine or acid functionalities and a well-defined number of azide groups on the surface. After deprotection, the dendrimers can be bifunctionalized in an orthogonal fashion by using 'click' chemistry to attach one functional group onto the dendrimer and using standard ester or amide formation protocols or thiurea linkages for the second functionalization giving us the unique possibility to bifunctionalize dendrimers for biological applications in a predesigned and well-controlled manner.[101,105,141,142,162-164,167,171,172,183,185] It is important to note that this methodology could also allow for triple surface functionalization by first using 'click' chemistry followed by a difunctionalization of the remaining surface functionalities using the stoichiometric difunctionalization strategy outlined in Figure 10B. While Dr. Weck is an expert in supramolecular chemistry and will direct all dendrimer synthesis, we are fortunate to have Dr. Bunz as a consultant. An expert in 'click' chemistry, Dr. Bunz has already made a 'clickable' biotin in gram quantities for binding to avidin fusion proteins (Aim II).

For our initial studies, we will synthesize dendrimers using a) ethylene-*d4*-diamine as the core followed by standard divergent dendrimer synthesis to yield the final amine functionalized dendrimer and b) **Core 4** which will be functionalized with four dendrons (three dendrons containing ONLY surface acid functionalities and one dendron which is based on MFCBU **1**) using the convergent dendrimer approach to give a bifunctionalized dendrimer that contains only one terminal alcohol moiety. These two dendrimers will allow us to study the monofunctionalization strategy as well as acetylenes and C-D Raman labels. At a later stage of the project, we will target the synthesis of dendrimers containing all proposed cores and dendrons.

I.B. Correlation among nanocluster size and Raman vs. fluorescence excitation spectra. Based on our preliminary results on nanodot fabrication, we will employ the diverse PAMAM-based materials to further optimize conditions to produce nearly pure, highly fluorescent nanodot solutions of desired excitation and emission colors. For a given dendrimer, this optimization will be performed systematically in 96-well microtiter plates. For example, dendrimer and metal ion concentrations will by changed along each axis to assay differences in nanodot creation and fluorescence or Raman stabilization. Each well within the microtiter plates will be directly read with the fluorescent plate reader available at Georgia Tech to generate excitation and emission spectra for all sets of creation conditions. This spectroscopic information will be correlated with ESI mass spectrometric investigations of nanocluster size. Together these studies will fully characterize nanodot samples and the size and scaffold dependence of their emission. Identical studies will be performed on each modular dendrimer type synthesized. Optical properties on both the bulk and single molecule level will be characterized to determine optimal fluorescence excitation and Raman excitation wavelengths. Furthermore, the excitation strengths and quantum yields can be determined from these solutions. Additionally, as SM-Raman is strongly correlated with strong nanocluster fluorescence, small aliquots from optimized fluorescent nanodot creation conditions will be diluted to measure the absorption cross-sections, emission rates and Raman peak frequencies and relative strengths on the single molecule level. Measuring optical properties for statistically significant properties of single molecules obviates the need to know bulk concentrations. Such experiments are routinely done in the Dickson lab through either confocal or total internal reflection laser excitation through a 1.4 NA 100x microscope objective. Either single element fiber coupled APD or MCP-PMT photodetectors are used to detect emission or one of several high sensitivity CCD cameras are used to image a large field of view. Typically for spectroscopy, an image is taken through the monochrometer attached to the side port of one of our Olympus IX70 inverted microscopes. In imaging mode, a mirror is used in place of a grating. Then the monochrometer slits are inserted and grating rotated into place, thereby producing spectra of the single molecules/nanoclusters previously observed to be between the slits in the initial image. This instrument simultaneously gives wide-field fast imaging capability, blinking and lifetime measurements and complete spectral characterization of SM-Raman and fluorescence of several features at once. All such detailed single molecule characterizations will be performed on nanodots optimized via the creation methods above.

SM-Raman studies. Because the Raman enhancement is a local effect, controlled Raman tag placement within the dendrimer will identify the position of the nanocluster within each dendrimer based on the specific vibrational transitions it enhances. By studying the

Raman signal of C-D bonds (~2050 cm^{-1}) placed in different shells according to the synthetic procedure above, we can understand the position of the nanocluster within the dendrimer core and how to further improve the optical signal. Optimization of the Raman signals should then enable more vibrational modes to be incorporated, thereby creating even stronger emissive labels. As Raman is an instantaneous inelastic scattering process, it has an extremely fast lifetime component (<100 fs) and is therefore very strong and narrow compared with fluorescence. Using time correlated single photon counting (tcspc) to determine relative contributions from fluorescence and Raman at each wavelength, we will directly determine the optimal excitation wavelengths for each color of Ag and Au nanoclusters to optimize the unique Raman signals. Furthermore, by using available equipment in the Dickson lab, lifetime measurements down to 10 ps both in bulk and on single nanodots are possible and routinely performed. The extremely fast lifetime provides yet another important sensitivity enhancement opportunity. By gating the detection to only collect the strongly emitting fast component (with our photon counting apparatus, and for entire fields of view with a LaVision gated CCD with 200ps time resolution to be purchased with cost sharing as part of our center for optical microscopy), we can complete discriminate against typical nsec lifetime background fluorescence to isolate the nanocluster fast fluorescence (Ag) and Raman components, or for Au, just the instantaneous Raman component. This time discrimination will greatly enhance the sensitivity and enable in vivo single molecule imaging with our unique nanodots. Together with the previously measured fluorescence quantum yields, we can truly optimize the excitation wavelengths to preferentially produce the Raman and fluorescence signals of interest.

Fluorescence stability. Largely unaffected by environmental interactions, the dendrimer-stabilized emission will be further explored to yield quantitatively similar emission for a given nanodot in a wide variety of different environs. Such environmental insensitivity is in stark contrast to that of II-VI (e.g. CdSe) quantum dots in which surface passivation is crucial to overall photophysical properties due to the presence of trap states on the surface.[10,11,52,189-191] The dendrimer-encapsulated nanodots appear to circumvent such difficulties by having the chromophore ensconced within the water-soluble dendrimer core. We will directly probe the blinking (fluorescence intermittency) as a function of ionic strength and pH. Commonly used buffers such as phosphate buffers and sodium acetate/acetic acid will be used to simultaneously control pH while adjusting ionic strength. Although we have seen minimal photobleaching from Ag nanodots, even after hours of continuous emission and $>10^{11}$ photons emitted from most individual nanodots, we will assay the photobleaching quantum yields and characterize nanodot blinking dynamics under a wide range of conditions. In addition to blinking and total emission intensity, the fluorescence lifetime and spectra will also be measured to assay whether any changes occur due to environmental interactions. This is all conveniently done with time-tagged photon-by-photon[192,193] analysis possible with our tcspc setup. Both bulk and single molecule experiments will be performed to decipher if any change in photophysical dynamics results from altered blinking dynamics or an average overall reduction in fluorescence efficiency.

Specific Aim II. Build and assay biological specificity.

Rationale: Targeted delivery of molecules into live cells is the focal point of current research in drug delivery and gene therapy. The hydrophobic character of the plasma membrane effectively seals the cytoplasm from the extracellular milieu. Only moderately hydrophobic compounds of low molecular weight undergo rapid passive diffusion across the cellular membrane. An increasing number of methods are being developed to enhance uptake of poorly permeable molecules.[194-203] The perhaps most successful methods are based on conjugates of short peptide sequences, which were adapted from viral proteins.[204] Another approach aims to harness the polyamine transporter PAT,[205] a cell surface protein which is responsible for the uptake of polyamines required for cell growth. Recently a synthetic receptor targeting strategy has been developed, which was originally inspired by the clathrin-mediated endocytosis of cholera toxin.[206-209] The dendrimer framework provides an extremely versatile platform to design poly-functionalized nanodots. Chemicals tags, which are designed to enhance cellular uptake can be readily combined with a variety of peptide sequences to specifically target subcellular locations or organelles. The overall goal, efficient cellular uptake and target-specific labeling of proteins with dendrimer nanodot conjugates, will be approached sequentially, largely in the Fahrni lab. First, we will study the uptake efficiency as a function of various chemical tags grafted onto the dendrimer surface. Second, we will synthesize bifunctional dendrimer conjugates, which combine the most efficient modifiers with a small ligand for fusion protein labeling. The dendrimer framework will be functionalized with the cellular uptake modifier and combined with either biotin or O^6-benzylguanidine (BG) as the fusion protein ligand.

Experimental Approach

II.A. Target-specific functionalization of dendrimer-encapsulated nanodotsTwo basic classes of side-chains are proposed for dendrimer functionalization: a) synthetic membrane transporting molecules and b) biorecognition motifs for specific binding to the protein of interest. As outlined above, for efficient synthesis, screening, and *in vivo* evaluation of the dendrimer derivatives, the side-chains will be attached through general 'click' coupling chemistry. Bifunctionalization of dendrimers with both membrane transporting and biorecognition motifs will be attached through orthogonal peptide- and click-coupling protocols, respectively.

1. Polyamine functionalization. At physiological pH PAMAM dendrimers are compact polycationic polymers, that effectively enhance the delivery of plasmid DNAs or oligonucleotides in live cell cultures.[114,149,154] Similarly, conjugates of drugs or DNA with polyamines such as sperimidine exhibit significantly enhanced uptake rates compared to their unconjugated analogues.[210,211] In both cases, the uptake is thought to be mediated by the polyamine transporter (PAT); however, the actual mechanism is poorly understood. The PAT system might be also responsive towards uptake of unfunctionalized PAMAM encapsulated nanodots, which form at neutral pH similar polycationic species. Many studies have demonstrated the uptake of PAMAM dendrimers and its utility in drug delivery. The number of protonated amino groups increases exponentially with the generation size of the dendrimer, and is thus, an important variable in probing uptake efficiency. In addition, structure-activity studies of polyamine-uptake *via* the PAT system revealed that the spacing between the positively charged amino-groups is critical to their activity. Key-parameters to be optimized include therefore, the

spacer-lengths (n, m) in PA_{nm} as well as the number of polyamine-side terminators attached to the dendrimer. Using the already published activity relationships as guideline,[210,211] we will focus primarily on the most effective polyamine modifiers.

Cell culture experiments. The uptake efficiency of nanodots will be measured at various incubation times with near-IR fluorescing Au_{23} nanodots, with cell suspensions being analyzed by flow cytometry and normalized against propidium iodide as an internal standard.[212] The technique will be used also to determine the uptake kinetics and its dependence on the probe concentration. To gauge organism- and tissue-specific influences on the translocation efficiency, we will perform the uptake experiments with several different mammalian cell lines, including human HeLa and HepG2 cells, 3T3 mouse fibroblast cells, and CHO cells. Cytotoxicity will be evaluated by estimating the cell viability by dye uptake.[213] Viable cells take up diacetyl fluorescein and hydrolyze it to fluorescein, which is cell impermeable and in a completely different spectral region from our Au_{23} nanodots. The population of viable cells can be measured via flow cytometry using again propidium iodide as internal standard.

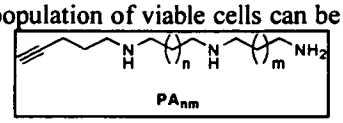

Synthetic Strategies. Polyamine functionalized dendrimers will be synthesized *via* 'click' chemistry from the corresponding azide-terminated dendrimers using various alkyne-functionalzied polyamines PA_{nm}. As pointed out above, this coupling method tolerates a wide range of functional groups and does not require protection of the primary or secondary amino groups. The precursors PA_{nm} will be synthesized *via* reductive amination of the ω-alkynyl aldehyde as described for similar polyamine derivatives.[214] The modular approach will allow us to synthesize and screen a wide range of polyamine-decorated dendrimers and therefore will guarantee rapid progress in evaluating the efficiency of this uptake strategy.

2. Functionalization with arginine-rich peptides. Several classes of water-soluble peptides have been identified that facilitate uptake across the plasma membrane of live cells and tissues.[204] For example, the peptide sequences found in HIV-tat, adenoviral RME, or in Antennapedia exhibit high translocation efficiencies.[198,215-218] The respective sequences of all three peptides consist of several basic residues forming a polycation at physiological pH. The portion of the Tat-peptide, which is critical for translocation across the membrane (RKKRRQRRR) contains six arginines and two lysines. Similarly, Atennapedia Antp-(43-58) is composed of three arginines and four lysines.[201,202,219-221] Inspired by the polycationic nature of these sequences, Wender and coworkers found that simple guanidinium-based oligomers are also efficient molecular transporters and exhibit often superior translocation activities compared to viral peptide sequences.[222,223] Internalization of these peptides proceeds typically within minutes even at 4°C,[224,225] and is not suppressed by endocytosis inhibitors,[226] thus clearly excluding the endocytosis pathway as the uptake mechanism. This observation is particularly important for *in vivo* labeling, because endocytosed nanodot conjugates would be caged inside vesicles unless they carry specific signaling tags to escape the endosomal/lysosomal pathway. Hence, we hypothesize that polyarigine-functionalization of the dendrimer-nanodot-conjugates may further increase the uptake efficiency compared to polyamine-mediated translocation. Again, uptake efficiency will be measured via flow cytometry using highly fluorescent Au nanodot solutions.

Alternate Approaches. The dendrimer surface functionalization is pivotal to increase the uptake efficiency; however, upon internalization the modifiers are not further required and could potentially give rise to undesired non-specific interactions. Using a hydrolyzable ester for the conjugation of the nanodot to the arginine-based transporters, release of the unconjugated label could be effectively controlled in a pH-dependent fashion.[227] Kirschberg *et al.* recently demonstrated that cellular uptake and subsequent release of taxol can be effectively controlled by pH-dependent cleavage of the ester linker with an amino-group attached in close proximity.[228] If necessary, this attractive strategy can be readily adapted to our system by converting the alcohol-terminated dendrimer to the corresponding chloroacetyl derivative followed by substitution with polyarginine modified with an N-terminal cystein residue (Scheme 1). The nucleophilicity of the proximal amino-group (bold) towards ester-cleavage can be readily adjusted and provides an effective way to tune the half-life of the conjugates from 1 to over 200 minutes (PBS, pH 7.4, 37°C).[228] The core-facility of the Petit Institute for Bioengineering and Bioscience at Georgia Tech houses a state-of-the-art solid-phase peptide synthesizer, which will allow us to synthesize the required peptide precursors in large quantities.

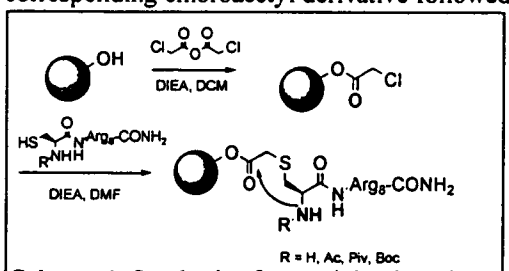

Scheme 1. Synthesis of an arginine-based transporter and it's controlled cleavage off the dendrimer.

II.B. Bifunctionalized dendrimer-encapsulated nanodots for *in vivo* protein labeling. By far the most successful strategy to study localization, interactions, and activities of proteins *in vitro* and *in vivo* is based on fusion proteins. In this approach the protein of interest is genetically engineered with a unique sequence (peptide or protein) at either the N or C terminus. Using an autofluorescent tag, such as the green fluorescent protein (GFP), high concentrations of the fusion protein can be observed in live cells without further fixation or labeling procedures.[229] Although this approach is currently the most powerful technique for *in vivo* studies, there are inherent limitations in single molecule applications. However, the fusion protein technique is principally suitable to label proteins with a non-biological fluorescent tag with improved photophysical properties.[230] In this strategy the tag-sequence binds either reversibly or through covalent bond modification to the small fluorescent molecule. Using avidin as the genetically encoded tag, the dendrimer-nanodot conjugate will be attached to the fusion protein *via* a biotin linker. The modular structure of the proposed dendrimers is well suited to design bifunctional conjugates, which combine peripheral functional groups for optimized cellular uptake with a *single* ligand for fusion protein binding.

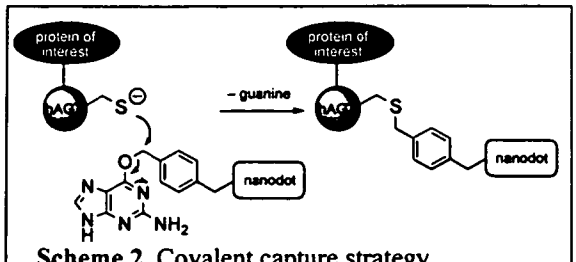

Scheme 2. Covalent capture strategy.

Expression of avidin or streptavidin fusion proteins in the cytosol can be toxic to the cell at very high expression levels, and the biotinylated nanodot conjugate has to compete with the endogenous cofactor for binding, thus potentially limiting the scope of the proposed approach. We will therefore also explore a complementary strategy recently developed by Johnsson *et al.* based on tag-mediated covalent bond formation between the fusion protein and its ligand.[231-233] This approach utilizes the reaction of the human DNA repair protein O^6-alkylguanine-DNA alkyltransferase (hAGT, 207 residues) with O^6-benzylguanine (BG) derivatives (Scheme 2). The normal function of hAGT is to repair O^6-alkylated guanine in DNA by transferring the alkyl group to a reactive cystein residue. The reaction of an hAGT fusion protein with BG derivatives leads therefore to covalent labeling via a stable thioether linkage. This approach does not depend on the nature of the label and should be also suitable for covalent attachment of nanodot conjugates. The reaction kinetics of the natural protein has been recently optimized *via* directed evolution providing versatile tools for efficient *in vivo* and *in vitro* labeling of hAGT fusion proteins.[233] The BG ligand will be conjugated to the dendrimer framework *via* a 'click' linker. At present, the irreversibility of the attachment chemistry combined with low toxicity of the labeling-ligand render this approach most attractive. However, the engineered hAGT tag will also compete with the endogeneous substrate, thus reducing either the labeling efficiency or requiring the use of hAGT deficient cell lines.

Synthetic Strategies. The alkyne-modified biotin **B1** required for coupling with the azide-terminated dendrimer is readily obtained via DCC-promoted amide-coupling of (D)-biotin with commercially available propargylamine. The alkyne-functionalized O^6-benzylguanine derivative **B2** is synthesized from *p*-aminomethyl-benzylguanine as described for similar conjugates.[233] The corresponding carboxylic acid precursor is obtained *via* reaction of glutaric anhydride with propoargylamine (Scheme 3).

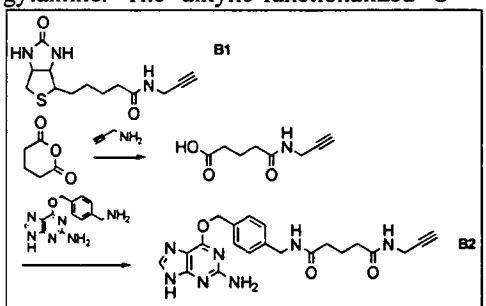

Scheme 3. Synthesis of acetylene-containing biospecific moieties.

Confirmation of labeling efficiency and probe brightness upon conjugation. Nanodots will be formed both prior to and after 'click' chemical functionalization. While 'click' chemistry is very tolerant of other chemical groups, we will likely first modify the PAMAM surface and subsequently determine optimal chemical conditions for producing each nanodot color with different functionalities. Using our single molecule and bulk methods, we will characterize nanodot brightness, fluorescence lifetimes, quantum yields, blinking dynamics and any shifts in Raman transitions upon attaching additional functionality to the PAMAM surface. Together, these will confirm that the nanodot optical properties are independent of attachment and suitable for further biofunctionalization.

Alternative Approach. An alternative method for dendrimer-nanocluster translocation across the cytoplasmic membrane is the "Pro-Ject Protein transfection reagent" available from Pierce. The Pro-Ject reagent, a cationic lipid formulation, has been shown to deliver biologically active proteins such as GFP and β-galactosidase, peptides, antibodies, or dextran sulfate into living cells [234-236]. At least twelve different cell lines have been tested successfully. This delivery system will be tested with biotin- or BG- mono-functionalized dendrimer derivatives to assay whether the nanoclusters are efficiently transported into cells in an analogous manner.

Specific Aim III. Intracellular single molecule labeling, specificities and protein dynamics.

Rationale: Specific Aims 1 and 2 outline the synthetic methodology for creation and target-specific funtionalization of the modular nanodot conjugates. In Specific Aim III, we will further refine and expand the conjugation schemes to create much smaller biorecognition motifs for *in vivo* labeling using monofunctionalized nanodots prepared in Aim II to minimize steric perturbations imposed by the genetically encoded tag. We will subsequently test and evaluate the various labeling strategies on purified proteins *in vitro* and identify potential changes in the photophysical and biochemical properties of the resulting nanodot-protein hybrids. Finally, to study the suitability of the developed dendrimer-nanodot conjugates as *in vivo* labels in imaging protein dynamics and trafficking in live cells, we will label, gate, and monitor the differential subcellular localization of the human progesterone receptor in mammalian cells.[237] The diversity in biological specificity of these conjugation methods should enable generalized genetically encoded multicolor labeling of proteins of interest, thus greatly streamlining the *in vivo* imaging process and yielding single molecule sensitivity. Thus, through this Aim, we will develop novel methods for directly observing nanodot-protein conjugates on the single molecule level. utilize the strong fluorescence and lamp-based screening methods to identify specific peptides within bacteria-based libraries for strong nanodot fluorescence. This Specific Aim will therefore not only focus on the evaluation of the developed label in a biological environment, but push for new strategies to create genetically encoded domains that "capture" and directly image the ultrabright, membrane permeable single molecule probes, even in the presence of strong autofluorescence.

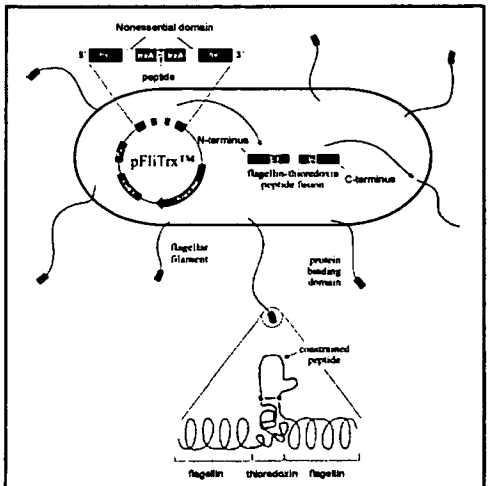

Figure 14. *E. coli*-based FliTrx peptide display method.

Experimental approach.

III.A. Identify specific, physically small, genetically encoded, protein-nanodot conjugation schemes. To further reduce the size of the *in vivo* label, we will employ a solution based screening strategy that combines an *E. coli* based peptide library[238,239] (FliTrx random peptide display library, Invitrogen) with fluorescence-activated cell sorting (FACS) to identify short peptide sequences with strong binding specificity to the nanodot target. Peptides that bind the target nanodots will be incorporated into proteins to bind the label *in vivo*. For example, we will screen libraries for binding to the Trojan peptide, a 16-amino acid α helix that mediates membrane

transport. This peptide will be used (Aim II) as one of the membrane transport methods for monofunctionalized nanodots and provides an excellent biorecognition motif, even when attached to the PAMAM dendrimer. In this approach the peptide modifier serves a dual function, being responsible for cellular uptake and binding to the genetically encoded tag. Identification of such binding peptides, much smaller than avidin and hAGT, will greatly enhance the utility of our dendrimer nonodots as versatile *in vivo* labels.

The FliTrx peptide library displays peptides on the surface of *E. coli* using the major bacterial flagellar protein (FliC) modified to contain a thioredoxin (TrxA) with random dodecapeptide insertions in its active site loop (Figure 14).[240,241] The random dodecapeptides are constrained by a disulfide bond formed within TrxA.[241] After tryptophan induction to ensure simultaneous display of all peptide fusions, the flagellin fusion protein is exported and assembled into flagella on the bacterial cell surface, displaying the constrained peptide (Figure 14). Libraries of random dodecapeptides displayed on the bacterial surfaces will be evaluated for binding to chemically modified nanodots. The population of bacteria will be sorted according to the fluorescence properties with flow cytometry to collect those bacteria generating the strongest fluorescence (Figure 15).

We will initially use a commercial display library (Invitrogen) that contains a diversity of 1.8×10^8 to identify peptide sequences that interact specifically with peptide-conjugated nanodots. Flow cytometry directly correlates cell/particle size with fluorescence that specifies the bacterial population for sorting using FACS. The collected bacteria will be plated out to isolate single colonies and the binding peptide sequence determined. The consensus peptide sequence will be expressed as an N-terminal fusion protein with the progesterone hormone receptor described below. In the unlikely event of the commercial library screening not revealing any nanodot binding sequences, we will generate the flagellin display libraries with different peptide lengths using the pFliTrx vector and oligonucleotides ranging from 27 bp to 90 bp cloned into the pFliTrx vector. The plasmids isolated from the collection of clones will then be transformed and screened as described above.

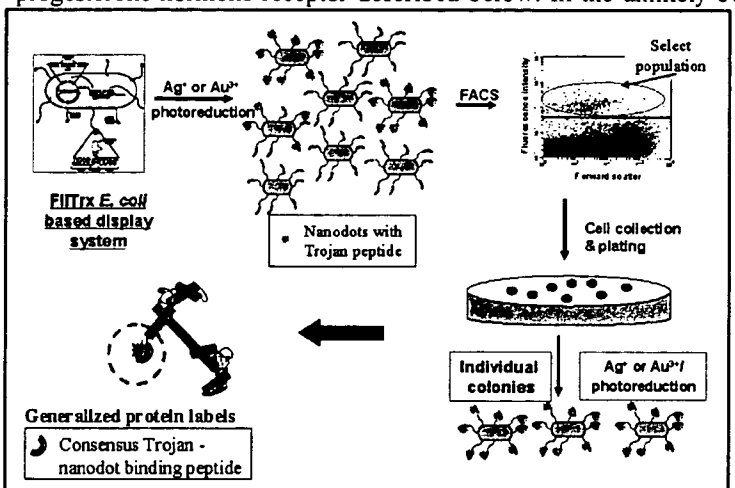

Figure 15. Peptide library screening scheme to identify genetically encodable Trojan peptide/nanodot binding peptides.

Potential difficulties and alternative approaches. We have found that both Ag and Au nanodots are very stable and retain their very bright fluorescence at physiological NaCl concentrations. Because flow cytometry can select cells based on scatter and fluorescence, the very small dendrimers will be undetectable in both channels. Only the cells are sufficiently large to scatter enough light to initiate collection, thereby avoiding false positives due to dendrimer-encapsulated nanodot fluorescence. Additionally, each bacterium within the FliTrx library has thousands of peptide copies, thus providing the potential for much stronger fluorescence signals. Only cells with strong fluorescence and scattered light will be collected, and characterized.

III.B. Test and optimize the suitability of these modified dendrimer nanodot conjugates for single molecule *in vivo* imaging of protein dynamics and trafficking. While even scrupulously prepared eukaryotic cells exhibit a great deal of autofluorescence, most "pure" solutions are too strongly fluorescent for practical single molecule imaging. Consequently, it is likely that a significant portion of the fluorescent background begins with the culture media. We will assay growth media and plates from many different companies for low level fluorescence to minimize the background fluorescence in single molecule imaging. After choosing the lowest background materials, we will photobleach all remaining fluorescent impurities with Hg-lamp illumination. Growth of cells in these photobleached media will be examined to ensure normal growth behavior. The optimal compromise in reducing background and cell viability will be reached to have cell cultures suitable for testing the toolbox components in the proposed *in vivo* single molecule studies.

1. In vitro studies. Prior to *in vivo* studies, all avidin and hAGT fusion proteins will be overexpressed, purified, and labeled with biotin- and BG- derivatized dendrimer nanodots, respectively, *in vitro* to characterize their biochemical and photophysical properties. The commercially available "Echo cloning system" (Invitrogen) will be adapted to enable cloning of genes into multiple expression systems for analysis. The Echo cloning system is a two-vector system that utilizes the Cre-lox site-specific recombination system of bacteriophage P1 for rapid, directional cloning from a single donor vector into multiple expression vectors.[242] Plasmids encoding avidin, human progesterone receptor and hAGT will be generous gifts of Dr. M. Kulomaa (University of Jyväskylä, Finland[243]), Dr. O'Malley (Baylor School of Medicine), and Dr. Johnsson (Switzerland), respectively. The avidin-KDEL will be made by PCR amplification with primer carrying the tetrapeptide coding sequence, while the avidin-$(GGS)_4$-PR, and the hAGT-$(GGS)_4$-PR constructs will be generated through overlapping extension PCR. For example, overlapping primers containing the linker sequence as well as 3′-avidin and 5′-PR coding sequences at the appropriate ends will be synthesized and used in the two-step PCR procedures to yield the avidin-$(GGS)_4$-PR fusion. This fusion construct will be cloned into the donor vector, pUni/V5-His-TOPO through the TOPO cloning method, and then recombined with acceptor vectors suitable for bacterial, insect, or mammalian expression[243-246]. The donor and acceptor vectors are incubated with Cre recombinase to generate a fusion of the two vectors to form a single functional expression vector and place the gene of interest downstream from the promoter and regulatory sequences of the acceptor vector. This versatile method will allow us to test various expression systems and identify the best system for producing sufficient recombinant fusion proteins for *in vitro* studies as well as generating the mammalian expression construct for *in vivo* studies.

Characterization of fusion protein-nanodot conjugates. After the fusion proteins are in hand, we will first determine whether the K_d between the avidin fusions and the biotin-dendrimer nanodots is similar to that reported for biotin-avidin interaction. A decrease in

K_d would suggest unfavorable interaction caused by the label that is readily ameliorated by changing the linker. The molar ratio for highest avidin-biotin complex and hAGT-BG adduct formation will also be defined under various pH, ionic strength, and cell lysate conditions. This information will be valuable in optimizing the *in vivo* studies. For all fusion proteins, the binding affinities will be measured by a combination of classical thermodynamic and kinetic methods as well as by fluorescence correlation spectroscopy. From three-dimensional orientation measurements of individual dye molecules,[31,133,137] we know the exact form of the microscope point spread function. Consequently, we can directly measure photons emitted from labeled and unlabeled molecules as they diffuse through the tight laser focus. The average residence time in the laser spot is a direct measure of the diffusion constant and therefore molecular mass.[247-252] This method will easily distinguish between conjugated and unconjugated nanodots and directly give the relative concentrations in solution. While the binding used for conjugation is extremely strong (in hAGT-BG a covalent bond is formed, while in biotin-avidin the K_d of the non-covalent interaction is $\sim 1 \times 10^{-15}$ M), it is expected that if the proper nanodot concentrations are used, essentially no unconjugated label will exist in solution. Relative total emission intensities will be determined to assure that conjugation with the protein does not diminish overall nanodot emission intensity. Additionally, using the very narrow and chemically/environmentally sensitive nanodot Raman spectrum, we may be able to see slight spectral shifts compared with free nanodots. Once nanocluster location within the dendrimer is known and Raman tags are placed in the appropriate places (Aim I), such a shift in vibrational frequency upon binding may be observable to clearly discriminate between bound and unbound nanodots. Although likely a small effect, especially for the ligand binding to the protein, deuterated biotin will also be 'clicked' onto the PAMAM scaffold to attempt measuring the Raman spectrum of the biotin tag.

2. In vivo studies. To test the biotin-linked dendrimer nanodot labels *in vivo*, two classes of fusion proteins will be constructed and examined in mammalian cells. First, as described in a study that examined interaction of fluorescein-biotin labels with avidin *in vivo,*[253] avidin will be simply appended with a C-terminal tetrapeptide, KDEL, a motif that directs proteins to the lumen of the *endoplasmatic reticulum* (ER). Cells transiently transfected with this avidin construct will then be incubated with bis-functionalized nanodots that are conjugated to biotin and a modifier to facilitate translocation across the plasma membrane (Aim II). By changing the incubation time and extracellular concentration of the nanodot labels we will systematically explore potential artifacts caused by unbound or non-specifically bound labels. The subcellular localization of the avidin construct will be visualized by immunofluorescence techniques using calreticulin as the ER marker. Once the avidin localization has been confirmed, we will determine whether the biotin-linked dendrimer nanodots efficiently penetrate and properly localize within avidin-containing subcellular compartments. Alternatively, the conjugation of biotinylated dendrimer with avidin-KDEL can be formed *in vitro* using purified avidin-KDEL and the complex subsequently transported across the membrane with the Pro Ject system, enabling the dynamics of *in vivo* trafficking to be monitored.

Gated dynamics of progesterone receptor proteins. Because subcellular localization is an area of active research not only in the field of nuclear receptors,[254] but also in investigating diseases such as leukemia[255] and cancer,[256] we will further evaluate the utility of the nanodot-conjugates to follow single molecule trafficking of the progesterone receptor (PR) in live mammalian cells. The avidin- and hAGT-PR fusion proteins will be transiently expressed in HeLa cells by transfecting with the corresponding plasmids. Avidin-linker-PR is comprised of avidin linked to the progesterone receptor through a $(GGS)_4$ linker that minimizes potential steric interference between the two functional domains.[257] Avidin binds biotin with very high affinity,[253] thereby providing an extremely slow off-rate kinetics of the nanodots attached to the fusion-protein. The progesterone receptor, in the absence of progesterone, is approximately evenly distributed between the cytosol and the nucleus. Addition of progesterone induces a conformational change which promotes trafficking of the receptor and translocation to the nucleus (Fig. 16), resulting in a distribution heavily in favor of the nucleus. This system has been extensively studied in live cells using PR-GFP fusion proteins.[237] While allowing determination of the localization of the progesterone receptor, the GFP label can not provide information on the redistribution kinetics on a single molecule level. However, the nanodot conjugate single-molecule labels overcomes this deficiency, thereby enabling dynamics of progesterone-dependent trafficking of the nuclear receptor to be directly imaged, *in vivo.* Furthermore, this progesterone-dependent system will allow us to quantify the amount of unbound label that remains in the cytosol, and thus optimize delivery conditions to achieve the highest possible signal to noise ratio. Additionally, adjusting the nanodot and progesterone concentrations outside the cell will enable intracellular single molecule concentrations to be readily observed. The 'steady state' distribution of progesterone receptor will be independently determined through immunofluorescence experiments, and correlate with the data obtained with dendrimer nanodots (see below). In addition, the demonstration of progesterone triggered trafficking will confirm proper folding of all structural domains within the fusion proteins, an important prerequisite for *in vivo* label delivery and target conjugation. Using the same strategy, we will also explore the attachment of the nanodot conjugate via covalent linkage to the corresponding hAGT fusion protein as outlined in Specific Aim II and with the much smaller consensus peptide recognizing the Trojan peptide-nanodot conjugate..

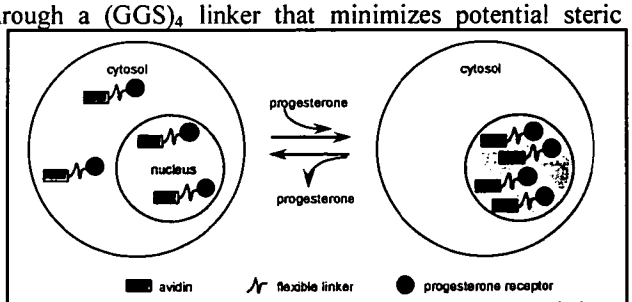

Figure 16. In the absence of progesterone, the avidin-linker-PR fusion protein is evenly distributed between the cytosol and the nucleus. When progesterone is added to the media, it binds the PR which dissociates from heat shock proteins in the cytosol, and moves to the nucleus. If the growth medium is replaced by growth medium without progesterone, the original distribution of the fusion protein between the cytosol and nucleus is restored.

Optical characterization of protein dynamics inside living systems on the single molecule level. Due to the very high background present in live cell imaging, we will utilize a variety of methods to isolate the bright emission from our noble metal nanodots. Already ~100x brighter than either CdSe or organic fluorophores and more robust, identifying optical signatures from individual nanodots on

top of a bright background will be challenging. Due to our close interaction with the Center for Advanced Research in Optical Microscopy at Georgia Tech, we will purchase a gated, intensified CCD camera (cost sharing from Georgia Tech) to collect only the emission within the first ~100 ps of our Ti:sapphire laser pulse. Combined with reduction our laser repetition rate to ~4MHz, gating will enable high efficiency collection only of the fast components of the nanodot fluorescence and Raman emission and effectively filter out all longer lasting autofluorescence. Images obtained in this manner will improve the s/n ratio by at least an additional factor of 50. Using a narrow band emission filter that only passes the Raman emission from the incorporated vibrational labels will further decrease the background. Together using the time and frequency selective methods enabled by imaging our strongly emitting nanodots, we should be able to directly view dynamics of individual proteins in living eukaryotic cells within the time frame of this proposal.

Intracellular diffusion measurements. While the gated flow of intracellularly labeled protein into the nucleus will confirm that proteins were labeled within the cytosol, the powerful control system of the progesterone receptor enables us to compare diffusion constants of individual proteins within living cells. In addition to time-gated imaging, we will use a photon-by-photon approach with our tcspc board to perform autocorrelations of emitted photons.[192,193] As we collect the raw data, we can combine the pulsed excitation and well-known point spread function of our excitation source to determine diffusion constants intracellularly. As the diffusion constant for our emissive nanodot and the nanodot conjugated to the protein of interest will be very different, these intracellular fluorescence correlation spectroscopy (FCS) measurements will provide independent confirmation of nanodot conjugation to the progesterone receptor. While all photophysical properties will be characterized on the single molecule level when conjugated to the progesterone receptor. These measured intracellular diffusion constants will also be compared to those for the identical *in vitro* system.

Potential difficulties and alternative approaches. The progesterone receptor has been overexpressed in both bacteria and insect cells,[258] whereas bacterial,[245,246], insect, and mammalian[244] expression systems have been developed for avidin. Consequently, we expect to obtain sufficient recombinant protein material for *in vitro* characterization. In addition, several studies have demonstrated that avidin chimeras can be labeled *in vivo* with membrane permeable biotinylated fluorescent dyes [253,259]. Similar *in vivo* experiments will be conducted as a parallel comparison between our dendrimer nanodots and organic fluorescent dyes. Given the chemical complexity of the intracellular environment, it is critical to carefully study and identify potential artifacts due to non-specific interactions of the probe with proteins, the lipid bilayer of vesicles or organelles, and other cellular structures or biomolecules. Among the multitude of possibilities lysosomes and acidic vesicles have been found to be the primary target for translocation and ultimately accumulation of drugs and non-natural molecules. Colocalization with acidic vesicles or lysosomes can be readily tested using the commercially available lysotracker probe or DAMP in combination with a fluorescein-labeled anti-dintrophenyl rabbit antibody. The gated transport of labeled progesterone receptors into the nucleus, however, will provide an unambiguous demonstration of the *in vivo* single molecule labeling and detection strategies detailed in this proposal.

Qualifications and synergies among assembled team. This project is inherently multidisciplinary. The assembled team consists of experts in single molecule microscopy, optical instrumentation, image analysis, and nanodot creation and photophysics (Dickson), dendrimer and organic synthesis (Weck), conjugation chemistry *via* Click chemistry (Weck, Bunz, Fahrni), membrane uptake, intracellular metal sensing, and live eukaryotic cell imaging (Fahrni), *in vitro* protein kinetics, bacterial expression, protein biochemistry, and library screening (Tzeng), and nuclear targeting, nuclear hormone receptor biochemistry, cell biology, and controlling nuclear transport and protein expression in eukaryotes with small molecule ligands (Doyle). While each investigator has his/her area of expertise, each Co-PI is very broadly trained, leading to very productive scientific overlap and fostering great creativity and insight into experimental methods and future directions. Combined with Dickson's preliminary results on dendrimer encapsulation and spectroscopy of single metal nanoclusters, the assembled group will collectively optimize the dendrimer chemical structure to create modular ultrabright nanodots with unparalleled Raman and fluorescence activity that readily cross cell membranes and specifically label the protein of interest in the cytoplasm. These materials will then be gated into the nucleus by small molecules to assess the efficiency of transport and binding. Through a combined chemical, optical, and biochemical approach, we will develop the necessary tools for *in vivo* labeling and high sensitivity tracking of individual proteins within living cells, even in the presence of high autofluorescent backgrounds characteristic of cellular media.

All investigators are in the Atlanta area, thereby facilitating greater interaction. Drs. Tzeng and Dickson are already jointly active in studying the optical properties of individual nanodots and demonstrating their *in vitro* labeling potential by very different means. In contrast, the proposed research focuses on dendrimer chemistry for Raman and fluorescence from Ag and Au nanoclusters and the dendrimer's modularity in conjugation chemistry. The additional focus on *in vivo* binding, cellular imaging and developing the necessary optical methods to create and characterize both sub-nm Raman and fluorescence based single molecule probes of unprecedented brightness and photostability offers tools that both improve upon and complement all other methods. Drs. Fahrni and Dickson continue their interaction on studying PAMAM uptake in different cell lines to assess the efficiency of nanodot labeling. It is an exciting and natural extension for Drs. Weck, Bunz, and Fahrni to combine their synthetic expertise to create new dendritic materials with novel Raman tags in background free spectral windows as well as attaching modular conjugation elements for highly specific membrane transport and protein labeling/recognition units. The specific targeting enabled with Dr. Doyle's expertise in nuclear signaling and hormone receptors completes the package necessary to label proteins within any region of the cell. This level of chemical and biochemical control and feedback/interactions among investigators is ideal for developing already existing, but improvable, nanodots that provide 100x increased sensitivity over current methods into unprecedented *in vivo* single molecule labels.

Each Aim requires the participation of multiple members, but all work will be conducted in parallel. Dr. Weck has already begun synthesizing dendrimers with Raman tags incorporated inside. While these internal changes and the mono, bis, and tri-functionalized dendrimers are being synthesized, Dr. Dickson will continue with optical characterization and solution preparation of Ag and Au nanodots on the single molecule and bulk levels. As PAMAM dendrimers are known to cross cell membranes, Dr. Fahrni will

investigate cellular uptake as a function of commercially available non-functionalized PAMAM generations. This will be readily visualized with the bright fluorescence from noble metal nanodots under Hg-lamp excitation through a standard fluorescence microscope. Concurrently, Drs. Doyle and Tzeng will overexpress, purify and characterize the progesterone receptor and its fusion with avidin. Dr. Bunz has already synthesized biotin attached to acetylene – perfect for dendrimer attachment through 'click' chemistry. As various agents are attached to the modular nanodot, Dr. Dickson will continue with optical characterizations such that the *in vivo* experiments are well-understood. Communication, transfer of materials, and *in vitro* characterization (optical, chemical and biochemical) will all be performed in parallel throughout the scope of the project. Materials will be transferred at monthly meetings, if not before. However, all investigators have already begun on different aspects of the project and will continue working and discussing progress toward our collective goal of tracking intracellular single molecule dynamics. These efforts will continue well beyond the 4-year scope of this proposal.

Coordination of efforts. We have obtained a cost sharing commitment ($30,000/year) from Georgia Tech's Administration for secretarial support of the proposed Exploratory Center. This will be tied into the Center for Advanced Research in Optical Microscopy (CAROM), of which Dr. Dickson is a Director. With seed funding from Georgia Tech's Administration, one primary goal of CAROM is to develop and make available new fluorescent probes with novel labeling and optical properties. Upon funding of this Exploratory Center application, CAROM will purchase a psec-gated intensified CCD camera (PicoStar HR, LaVision, Inc.) to directly image the nanodot Raman emission and fast fluorescence, devoid of the autofluorescent background – an extra $70,000 of cost sharing from Georgia Tech to benefit both centers. The tools demonstrated through this proposed work will be complemented by the resources of CAROM to demonstrate their utility in live cell imaging. All team members will have direct access to the developed tools and can reserve the Center's microscopes for live cell imaging. It is our plan to leverage these *in vivo* labeling tools to foster increased collaboration and understanding of a wide range of biological systems. CAROM is an excellent outlet for fostering future interactions and its goals are fully endorsed by the University.

As director of CAROM and developer of the first generation of nanodots for single molecule microscopy, Dr. Dickson will serve as the project director of this Exploratory Center. We have already scheduled joint monthly meetings to be on the first Wednesday evening of each month. These meetings will be specifically to address issues involved in the students' and postdocs' progress in all aspects of the project. Additionally, three of the graduate students and one postdoc on this project will be jointly supervised (Students supervised by: Weck/Fahrni, Fahrni/Doyle, and Dickson/Tzeng; Postdoc jointly supervised by Tzeng/Doyle) and will participate in independent monthly joint group meetings between the respective groups. The synergy among the investigators will lead to extremely productive discussions and problem solving through these meetings. Currently the School of Chemistry and Biochemistry has committed funds to CAROM for a seminar series in optical microscopy. As the establishment of this Exploratory Center is in line with future goals of CAROM, four of these monthly seminars will be devoted to bring in researchers involved in *in vivo* and *in vitro* imaging of single protein dynamics. This commitment from Chemistry and Biochemistry will facilitate further advances in our own chemistry, biochemistry, and imaging, as well as educate our students and advertise their work and the Exploratory Center itself. The administrative support promised upon the funding of this proposal will be utilized to advertise the center and encourage use of developed materials, once demonstrated for *in vivo* use. The assistant will also coordinate reports, meetings, seminars, purchasing, accounting, and exploratory collaborations. Throughout the project, as materials become available, all requests for modular materials and/or 'clickable' linkers will be processed through the center's administrative assistant.

Sequence of investigation: Although the implications of the proposed chromophore development and *in vivo* labeling and characterization extends well beyond the four years requested to complete the studies in this application, the proposed studies will create the proposed modular, specific, targeted single molecule biolabels with unprecedented brightness and potentially chemical specificity.

Timetable	Year 1	2	3	4
Specific Aim I – Create modular single molecule fluorescence and Rman probes				
A. Dendrimer design and synthesis	x	x	x	
Correlation among nanocluster size and Raman vs. fluorescence excitation spectra	x	x	x	x
Specific Aim II – Build and assay biological specificity				
A. Target-specific functionalization of dendrimer nanodots	x	x	x	
B. Bis-functionalized dendrimer nanodots for *in vivo* protein labeling		x	x	x
Specific Aim III – Intracellular single molecule labeling, specificities and protein dynamics.				
A. Identify specific tag binding genetically encoded peptide sequence through random peptide display libraries		x	x	x
B. Test and optimize the suitability of dendrimer nanodots for single molecule *in vivo* imaging of protein dynamics		x	x	x

Gender and Minority Issues: N/A
Human Subjects: N/A
Biosafety: None of the proposed compounds or proteins are known to have any toxicity. No pathogens will be used in these studies.
Vertebrate Animals: N/A

G. Literature Cited.

1. Lu, H. P. *et al.* Single-molecule enzymatic dynamics. *Science* **282**, 1877-1882 (1998).
2. Dickson, R. M. *et al.* On/off blinking and switching behaviour of single molecules of green fluorescent protein. *Nature* **388**, 355-358 (1997).
3. Peyser, L. A. *et al.* Photoactivated fluorescence from individual silver nanoclusters. *Science* **291**, 103-106 (2001).
4. Zheng, J. & Dickson, R. M. Individual water-soluble dendrimer-encapsulated silver nanodot fluorescence. *J. Am. Chem. Soc.* **124**, 13982-13983 (2002).
5. Peyser, L. A. *et al.* Mechanism of Ag_n Nanocluster Photoproduction from Silver Oxide Films. *J. Phys. Chem. B* **106**, 7725-7728 (2002).
6. Wilcoxon, J. P. *et al.* Photoluminescence from nanosize gold clusters. *J. Chem. Phys.* **108**, 9137-9143 (1998).
7. Bigioni, T. P. *et al.* Near-infrared luminescence from small gold nanocrystals. *J. Phys. Chem. B* **104**, 6983-6986 (2000).
8. Rabin, I. *et al.* Absorption spectra of small silver clusters Ag-n (n >= 3). *Chem. Phys. Lett.* **312**, 394-398 (1999).
9. Bonacic'-Koutecky, V. *et al.* Ab initio study of the absorption spectra of Ag_n (n=5–8) clusters. *J. Chem. Phys.* **115**, 10450-10460 (2001).
10. Bruchez, M. *et al.* Semiconductor nanocrystals as fluorescent biological labels. *Science* **281**, 2013-2016 (1998).
11. Chan, W. C. W. & Nie, S. M. Quantum dot bioconjugates for ultrasensitive nonisotopic detection. *Science* **281**, 2016-2018 (1998).
12. Kneipp, K. *et al.* Single molecule detection using surface-enhanced Raman scattering (SERS). *Phys. Rev. Lett.* **78**, 1667-1670 (1997).
13. Nie, S. M. & Emory, S. R. Probing single molecules and single nanoparticles by surface-enhanced Raman scattering. *Science* **275**, 1102-1106 (1997).
14. Michaels, A. M. *et al.* Surface enhanced Raman spectroscopy of individual rhodamine 6G molecules on large Ag nanocrystals. *J. Am. Chem. Soc.* **121**, 9932-9939 (1999).
15. Lai, J. C. *et al.* Single-cell measurements of polyamidoamine dendrimer binding. *Ann. Biomed. Eng.* **30**, 409-416 (2002).
16. Bielinska, A. U. *et al.* The interaction of plasmid DNA with polyamidoamine dendrimers: mechanism of complex formation and analysis of alterations induced in nuclease sensitivity and transcriptional activity of the complexed DNA. *Biochim. Biophys. Acta-Gene Struct. Expression* **1353**, 180-190 (1997).
17. Higashi, N. *et al.* Dendrimers with attached helical peptides. *Adv. Mater.* **12**, 1373-1375 (2000).
18. Mitchell, J. P. *et al.* A direct method for the formation of peptide and carbohydrate dendrimers. *Bioorg. Med. Chem. Lett.* **9**, 2785-2788 (1999).
19. Boas, U. *et al.* New dendrimer - Peptide host - Guest complexes: Towards dendrimers as peptide carriers. *Chembiochem* **3**, 433-439 (2002).
20. Zheng, J. *et al.* High quantum yield blue emission from water-soluble Au-8 nanodots. **125**, 7780-7781 (2003).
21. Funatsu, T. *et al.* Imaging of single fluorescent molecules and individual ATP turnovers by single myosin molecules in aqueous solution. *Nature* **374**, 555-59 (1995).
22. Ha, T. *et al.* Probing the interaction between two single molecules: Fluorescence resonance energy transfer between a single donor and a single acceptor. *Proc. Nat. Acad. Sci., USA* **93**, 6264-6268 (1996).
23. Vale, R. D. *et al.* Direct observation of single kinesin molecules moving along microtubules. *Nature* **380**, 451-453 (1996).
24. Deniz, A. A. *et al.* Single-molecule protein folding: Diffusion fluorescence resonance energy transfer studies of the denaturation of chymotrypsin inhibitor 2. *Proc. Natl. Acad. Sci. U. S. A.* **97**, 5179-5184 (2000).
25. Ha, T. J. *et al.* Single-molecule fluorescence spectroscopy of enzyme conformational dynamics and cleavage mechanism. *Proc. Natl. Acad. Sci. U. S. A.* **96**, 893-898 (1999).
26. Harada, Y. *et al.* Single-molecule imaging of RNA polymerase-DNA interactions in real time. *Biophys. J.* **76**, 709-715 (1999).
27. Kinosita, K. Stepping rotation is a protein machine revealed by single molecule imaging. *Biophys. J.* **78**, 149Wkshp (2000).
28. Dickson, R. M. *et al.* Three Dimensional Imaging of Single Molecules in Pores of Poly(acrylamide) Gels. *Science* **274**, 966-69 (1996).
29. Xie, X. S. Single-Molecule Spectroscopy and Dynamics at Room Temperature. *Acc. Chem. Res.* **29**, 598-606 (1996).
30. Lu, H. P. & Xie, X. S. Single-Molecule Spectral Fluctuations at Room Temperature. *Nature* **385**, 143-146 (1997).
31. Bartko, A. P. & Dickson, R. M. Three-Dimensional Orientations of Polymer-Bound Single Molecules. *J. Phys. Chem. B* **103**, 3053-3056 (1999).
32. Lu, H. P. & Xie, X. S. Single-molecule kinetics of interfacial electron transfer. *J. Phys. Chem. B* **101**, 2753-2757 (1997).
33. Hollars, C. W. & Dunn, R. C. Probing single molecule orientations in model lipid membranes with near-field scanning optical microscopy. *J. Chem. Phys.* **112**, 7822-7830 (2000).
34. Xie, X. S. & Lu, H. P. Single-molecule enzymology. *J. Biol. Chem.* **274**, 15967-15970 (1999).
35. Hu, D. H. *et al.* Single-molecule spectroscopy of the conjugated polymer MEH-PPV. *J. Am. Chem. Soc.* **121**, 6936-6937 (1999).
36. English, D. S. *et al.* Single-molecule spectroscopy in oxygen-depleted polymer films. *Chem. Phys. Lett.* **324**, 15-19 (2000).
37. Betzig, E. & Chichester, R. J. Single molecules observed by near-field scanning optical microscopy. *Science* **262**, 1422-1428 (1993).

38. Macklin, J. J. *et al.* Imaging and time-resolved spectroscopy of single molecules at an interface. *Science* **272**, 255-258 (1996).
39. Moerner, W. E. & Kador, L. Optical detection and spectroscopy of single molecules in a solid. *Phys. Rev. Lett.* **62**, 2535-38 (1989).
40. Orrit, M. & Bernard, J. Single pentacene molecules detected by fluorescence excitation in a p-terphenyl crystal. *Phys. Rev. Lett.* **65**, 2716-19 (1990).
41. Skinner, J. L. in *Single Molecule Optical Detection, Imaging, and Spectroscopy* (eds. Basché, T., Moerner, W. E., Orrit, M. & Wild, U. P.) (Verlag-Chemie, Munich, 1997).
42. Moerner, W. E. *et al.* Optical Probing of Single Molecules of Terrylene in a Shpolskii Matrix - A Two-State Single-Molecule Switch. *J. Phys. Chem.* **98**, 7382-89 (1994).
43. Yip, W. T. *et al.* Classifying the photophysical dynamics of single- and multiple- chromophoric molecules by single molecule spectroscopy. *J. Phys. Chem. A* **102**, 7564-7575 (1998).
44. Yanagida, T. *et al.* Single molecule analysis of the actomyosin motor. *Curr. Opin. Cell Biol.* **12**, 20-25 (2000).
45. Zhang, C. Y. *et al.* Quantum dot-labeled trichosanthin. *Analyst* **125**, 1029-1031 (2000).
46. Murray, C. B. *et al.* Synthesis and Structural Characterization of Ii-Vi Semiconductor Nanocrystallites (Quantum Dots). *Z. Phys. D-Atoms Mol. Clusters* **26**, S231-S233 (1993).
47. Murray, C. B. *et al.* Synthesis and Characterization of Nearly Monodisperse Cde (E = S, Se, Te) Semiconductor Nanocrystallites. *J. Am. Chem. Soc.* **115**, 8706-8715 (1993).
48. Peng, X. G. *et al.* Shape control of CdSe nanocrystals. *Nature* **404**, 59-61 (2000).
49. Rodriguez-Viejo, J. *et al.* Evidence of photo- and electrodarkening of (CdSe)ZnS quantum dot composites. *J. Appl. Phys.* **87**, 8526-8534 (2000).
50. Dabbousi, B. O. *et al.* (CdSe)ZnS core-shell quantum dots: Synthesis and characterization of a size series of highly luminescent nanocrystallites. *J. Phys. Chem. B* **101**, 9463-9475 (1997).
51. Nirmal, M. & Brus, L. Luminescence Photophysics in Semiconductor Nanocrystals. *Acc. Chem. Res.* **32**, 407-414 (1999).
52. Nirmal, M. *et al.* Fluorescence intermittency in single cadmium selenide nanocrystals. *Nature* **383**, 802-804 (1996).
53. Dubertret, B. *et al.* In vivo imaging of quantum dots encapsulated in phospholipid micelles. *Science* **298**, 1759-1762 (2002).
54. Jaiswal, J. K. *et al.* Long-term multiple color imaging of live cells using quantum dot bioconjugates. *Nat. Biotechnol.* **21**, 47-51 (2003).
55. Wu, X. Y. *et al.* Immunofluorescent labeling of cancer marker Her2 and other cellular targets with semiconductor quantum dots. *Nat. Biotechnol.* **21**, 41-46 (2003).
56. Sutherland, A. J. Quantum dots as luminescent probes in biological systems. *Curr. Opin. Solid State Mat. Sci.* **6**, 365-370 (2002).
57. Gao, X. H. *et al.* Quantum-dot nanocrystals for ultrasensitive biological labeling and multicolor optical encoding. *J. Biomed. Opt.* **7**, 532-537 (2002).
58. Mattoussi, H. *et al.* Self-assembly of CdSe-ZnS quantum dot bioconjugates using an engineered recombinant protein. *J. Am. Chem. Soc.* **122**, 12142-12150 (2000).
59. Heim, R. *et al.* Wavelength mutations and posttranslational autoxidation of green fluorescent protein. **91**, 12501-04 (1994).
60. Ormo, M. *et al.* Crystal Structure of the Aequorea victoria Green Fluorescent Protein. **273**, 1392-5 (1996).
61. Chattoraj, M. *et al.* Ultra-fast excited state dynamics in green fluorescent protein: Multiple states and proton transfer. **93**, 8362-67 (1996).
62. Brejc, K. *et al.* Structural basis for dual excitation and photoisomerization of the Aequorea victoria green fluorescent protein. **94**, 2306-11 (1997).
63. Cubitt, A. B. *et al.* Understanding, improving and using green fluorescent proteins. **20**, 448-55 (1995).
64. Kain, S. R. & Kitts, P. Expression and detection of green fluorescent protein (GFP). **63**, 305-24 (1997).
65. Malvezzi-Campeggi, F. *et al.* Light-induced flickering of DsRed provides evidence for distinct and interconvertible fluorescent states. *Biophys. J.* **81**, 1776-1785 (2001).
66. Garcia-Parajo, M. F. *et al.* Real-time light-driven dynamics of the fluorescence emission in single green fluorescent protein molecules. *Proc. Natl. Acad. Sci. U. S. A.* **97**, 7237-7242 (2000).
67. Cotlet, M. *et al.* Identification of different emitting species in the red fluorescent protein DsRed by means of ensemble and single- molecule spectroscopy. *Proc. Natl. Acad. Sci. U. S. A.* **98**, 14398-14403 (2001).
68. Lounis, B. *et al.* Photophysics of DsRed, a red fluorescent protein, from the ensemble to the single-molecule level. *J. Phys. Chem. B* **105**, 5048-5054 (2001).
69. Garcia-Parajo, M. F. *et al.* The nature of fluorescence emission in the red fluorescent protein DsRed, revealed by single-molecule detection. *Proc. Natl. Acad. Sci. U. S. A.* **98**, 14392-14397 (2001).
70. Garcia-Parajo, M. F. *et al.* Optical probing of single fluorescent molecules and proteins. *ChemPhysChem* **2**, 347-360 (2001).
71. Garcia-Parajo, M. F. *et al.* Looking at the photodynamics of individual fluorescent molecules and proteins. *Pure Appl. Chem.* **73**, 431-434 (2001).
72. Blum, C. *et al.* Single molecule fluorescence spectroscopy of mutants of the Discosoma red fluorescent protein DsRed. *Chem. Phys. Lett.* **362**, 355-361 (2002).
73. Gross, L. A. *et al.* The structure of the chromophore within DsRed, a red fluorescent protein from coral. *Proc. Natl. Acad. Sci. U. S. A.* **97**, 11990-11995 (2000).

74. Jakobs, S. *et al.* EGFP and DsRed expressing cultures of Escherichia coli imaged by confocal, two-photon and fluorescence lifetime microscopy. *FEBS Lett.* **479**, 131-135 (2000).
75. Wall, M. A. *et al.* The structural basis for red fluorescence in the tetrameric GFP homolog DsRed. *Nat. Struct. Biol.* **7**, 1133-1138 (2000).
76. Yarbrough, D. *et al.* Refined crystal structure of DsRed, a red fluorescent protein from coral, at 2.0-angstrom resolution. *Proc. Natl. Acad. Sci. U. S. A.* **98**, 462-467 (2001).
77. Verkhusha, V. V. *et al.* An enhanced mutant of red fluorescent protein DsRed for double labeling and developmental timer of neural fiber bundle formation. *J. Biol. Chem.* **276**, 29621-29624 (2001).
78. Sacchetti, A. *et al.* Oligomerization of DsRed is required for the generation of a functional red fluorescent chromophore. *FEBS Lett.* **525**, 13-19 (2002).
79. Empedocles, S. & Bawendi, M. Spectroscopy of Single CdSe Nanocrystallites. *Acc. Chem. Res.* **32**, 389-396 (1999).
80. El-Sayed, M. A. Some interesting properties of metals confined in time and nanometer space of different shapes. **34**, 257-264 (2001).
81. Link, S. *et al.* Transition from nanoparticle to molecular behavior: a femtosecond transient absorption study of a size-selected 28 atom gold cluster. **356**, 240-246 (2002).
82. Huang, T. & Murray, R. W. Visible luminescence of water-soluble monolayer- protected gold clusters. **105**, 12498-12502 (2001).
83. Fleischmann, M. *et al.* Raman spectra from electrode surfaces. *J. Chem. Soc. Chem. Comm.*, 80-81 (1973).
84. Fleischmann, M. *et al.* Raman spectra of pyridine at a silver electrode. *Chem. Phys. Lett.* **26**, 163-166 (1974).
85. Jeanmaire, D. L. & Van Duyne, R. P. Surface enhanced Raman spectroelectrochemistry part 1: Heterocyclic, aromatic and aliphatic amines adsorbed on the anodized silver electrode. *J. Electroanal. Chem.* **84**, 1-20 (1977).
86. Moskovits, M. Surface roughness and enhanced intensity of Raman scattering by molecules adsorbed on metals. *J. Chem. Phys.* **69**, 4159-4161 (1978).
87. King, F. W. *et al.* Theory of Raman scattering by molecules adsorbed on electrode surfaces. *J. Chem. Phys.* **69**, 4472-4481 (1978).
88. Hildebrandt, P. & Stockburger, M. Surface enhanced resonance Raman spectroscopy of rhodamine 6G adsorbed on colloidal silver. *J. Phys. Chem.* **88**, 5935-5944 (1984).
89. Weiss, A. & Haran, G. Time-dependent single-molecule Raman scattering as a probe of surface dynamics. *J. Phys. Chem. B* **105**, 12348-12354 (2001).
90. Mooradian, A. Photoluminescence from thin metal films. *Phys. Rev. Lett.* **148**, 873 (1969).
91. Moskovits, M. Surface-enhanced Raman spectroscopy. *Rev. Mod. Phys.* **57**, 783-824 (1985).
92. Kneipp, K. (2001).
93. Doering, W. E. & S., N. Single-Molecule and Single-Nanoparticle SERS: Examining the Roles of Surface Active Sites and Chemical Enhancement. *J. Phys. Chem. B* **106**, 311-317 (2002).
94. Cheng, J. X. *et al.* An epi-detected coherent anti-stokes raman scattering (E-CARS) microscope with high spectral resolution and high sensitivity. **105**, 1277-1280 (2001).
95. Chen, J. X. *et al.* Multiplex coherent anti-stokes Raman scattering microspectroscopy and study of lipid vesicles. **106**, 8493-8498 (2002).
96. Cheng, J. X. *et al.* Ordering of water molecules between phospholipid bilayers visualized by coherent anti-Stokes Raman scattering microscopy. **100**, 9826-9830 (2003).
97. Volkmer, A. *et al.* Time-resolved coherent anti-Stokes Raman scattering microscopy: Imaging based on Raman free induction decay. **80**, 1505-1507 (2002).
98. Cheng, J. X. *et al.* Laser-scanning coherent anti-stokes Raman scattering microscopy and applications to cell biology. **83**, 502-509 (2002).
99. Cheng, J. X. *et al.* Theoretical and experimental characterization of coherent anti-Stokes Raman scattering microscopy. **19**, 1363-1375 (2002).
100. Tomalia, D. A. Dendrimer Molecules. *Sci.Am.* **272**, 62-66 (1995).
101. Bosman, A. W. *et al.* About dendrimers: Structure, physical properties, and applications. *Chem. Rev.* **99**, 1665-1688 (1999).
102. Frechet, J. M. J. Dendrimers and supramolecular chemistry. *Proc. Natl. Acad. Sci. U. S. A.* **99**, 4782-4787 (2002).
103. Grayson, S. M. & Fréchet, J. M. J. Convergent Dendrons and Dendrimers: From Synthesis to Applications. **101**, 3819-1867 (2001).
104. Esfand, R. & Tomalia, D. A. Poly(amidoamine) (PAMAM) dendrimers: from biomimicry to drug delivery and biomedical applications. *Drug Discov. Today* **6**, 427-436 (2001).
105. Cloninger, M. J. Biological Applications of Dendrimers. **6**, 742-748 (2002).
106. Diederich, F. & Felber, B. Supramolecular chemistry of dendrimers with functional cores. *Proc. Natl. Acad. Sci. U. S. A.* **99**, 4778-4781 (2002).
107. Tomalia, D. A. Starburst Cascade Dendrimers - Fundamental Building-Blocks for a New Nanoscopic Chemistry Set. *Adv. Mater.* **6**, 529-539 (1994).
108. Dykes, G. M. Dendrimers: a review of their appeal and applications. *J. Chem. Technol. Biotechnol.* **76**, 903-918 (2001).

109. Crooks, R. M. *et al.* Dendrimer-encapsulated metal nanoparticles: Synthesis, characterization, and applications to catalysis. *Accounts Chem. Res.* **34**, 181-190 (2001).
110. Friggeri, A. *et al.* Chemistry on surface-confined molecules: An approach to anchor isolated functional units to surfaces. *J. Am. Chem. Soc.* **123**, 6388-6395 (2001).
111. Zheng, J. *et al.* Influence of pH on dendrimer-protected nanoparticles. *J. Phys. Chem. B* **106**, 1252-1255 (2002).
112. Torigoe, K. *et al.* Au(III)-PAMAM interaction and formation of Au-PAMAM nanocomposites in ethyl acetate. *J. Colloid Interface Sci.* **241**, 346-356 (2001).
113. Grohn, F. *et al.* Organization of hybrid dendrimer-inorganic nanoparticles on amphiphilic surfaces. *Macromolecules* **35**, 4852-4854 (2002).
114. Yoo, H. *et al.* PAMAM dendrimers as delivery agents for antisense oligonucleotides. **16**, 1799-1804 (1999).
115. Wiwattanapatapee, R. *et al.* Anionic PAMAM dendrimers rapidly cross adult rat intestine in vitro: A potential oral delivery system? *Pharm. Res.* **17**, 991-998 (2000).
116. Tripathi, P. K. *et al.* Dendrimer grafts for delivery of 5-flurouracil. *Pharmazie* **57**, 261-264 (2002).
117. Sanchez-Sancho, F. *et al.* Dendrimers as carrier protein mimetics for IgE antibody recognition. Synthesis and characterization of densely penicilloylated dendrimers. *Bioconjugate Chem.* **13**, 647-653 (2002).
118. DeLong, R. *et al.* Characterization of complexes of oligonucleotides with polyamidoamine starburst dendrimers and effects on intracellular delivery. *J. Pharm. Sci.* **86**, 762-764 (1997).
119. Gazumyan, A. *et al.* Novel anti-RSV dianionic dendrimer-like compounds: Design, synthesis and biological evaluation. *Curr. Pharm. Design* **6**, 525-546 (2000).
120. Kukowska-Latallo, J. F. *et al.* Intravascular and endobronchial DNA delivery to murine lung tissue using a novel, nonviral vector. *Hum. Gene Ther.* **11**, 1385-1395 (2000).
121. Matsunaga, S. *et al.* Clear visualization of the products of nonradioactive in situ hybridization in plant tissue by simple dark-field microscopy. *Micron* **28**, 185-187 (1997).
122. Bielinska, A. U. *et al.* Application of membrane-based dendrimer/DNA complexes for solid phase transfection in vitro and in vivo. *Biomaterials* **21**, 877-887 (2000).
123. Chen, C. Z. S. & Cooper, S. L. Interactions between dendrimer biocides and bacterial membranes. *Biomaterials* **23**, 3359-3368 (2002).
124. Sideratou, Z. *et al.* A novel dendrimeric "glue" for adhesion of phosphatidyl choline-based liposomes. *Langmuir* **18**, 5036-5039 (2002).
125. Luo, D. *et al.* Poly(ethylene glycol)-conjugated PAMAM dendrimer for biocompatible, high-efficiency DNA delivery. *Macromolecules* **35**, 3456-3462 (2002).
126. Florence, A. T. & Hussain, N. Transcytosis of nanoparticle and dendrimer delivery systems: evolving vistas. *Adv. Drug Deliv. Rev.* **50**, S69-S89 (2001).
127. Toth, I. *et al.* Novel cationic lipidic peptide dendrimer vectors - In vitro gene delivery. *STP Pharma Sci.* **9**, 93-99 (1999).
128. Lee, T. H. *et al.* Strongly enhanced field-dependent single-molecule electroluminescence. *Proc. Natl. Acad. Sci. U. S. A.* **99**, 10272-10275 (2002).
129. Sooklal, K. *et al.* A blue-emitting CdS/dendrimer nanocomposite. **10**, 1083-+ (1998).
130. Balogh, L. & Tomalia, D. A. Poly(amidoamine) dendrimer-templated nanocomposites. 1. Synthesis of zerovalent copper nanoclusters. *J. Am. Chem. Soc.* **120**, 7355-7356 (1998).
131. Djalali, R. *et al.* Au nanowire fabrication from sequenced histidine-rich peptide. *J. Am. Chem. Soc.* **124**, 13660-13661 (2002).
132. Slocik, J. M. *et al.* Monoclonal antibody recognition of histidine-rich peptide encapsulated nanoclusters. *Nano Lett.* **2**, 169-173 (2002).
133. Bartko, A. P. *et al.* Three-Dimensional Single Molecule Rotational Diffusion in Glassy State Polymer Films. *Phys. Rev. Lett.* **89**, 026101/1-026101/4 (2002).
134. Bartko, A. P. *et al.* Observation of dipolar emission patterns from isolated Eu3+:Y2O3 doped nanocrystals: New evidence for single ion luminescence. *Chem. Phys. Lett.* **358**, 459-465 (2002).
135. Lee, I. *et al.* Structural molecular dynamics studies on polyamidoamine dendrimers for a therapeutic application: Effects of pH and generation. *Macromolecules* **35**, 4510-4520 (2002).
136. Dickson, R. M. *et al.* Simultaneous imaging of individual molecules aligned both parallel and perpendicular to the optic axis. *Phys. Rev. Lett.* **81**, 5322-5325 (1998).
137. Bartko, A. P. & Dickson, R. M. Imaging three-dimensional single molecule orientations. *J. Phys. Chem. B* **103**, 11237-11241 (1999).
138. Peyser, L. A. *et al.* Harnessing Single Particle Dynamics in Silver Nanomaterials. *Proc. SPIE* **4636**, 81-87 (2002).
139. Ghosh, S. & Banthia, A. K. Towards fluorescence sensing polyamidoamine (PAMAM) dendritic architectures. *Tetrahedron Lett.* **43**, 6457-6459 (2002).
140. Kleinman, M. H. *et al.* Effect of protonation and PAMAM dendrimer size on the complexation and dynamic mobility of 2-naphthol. *J. Phys. Chem. B* **104**, 11472-11479 (2000).
141. Esfand, R. & Tomalia, D. A. Poly(amidoamine) (PAMAM) Dendrimers: from Biomimecry to Drug Delivery and Biomedical Applications. **6**, 427-436 (2001).

142. Thornton, A. *et al.* Novel Functionalized Poly(amido amine) (PAMAM) Dendrimers: Synthesis and Physical Properties. **30**, 7600-7603 (1997).
143. Tomalia, D. A. *et al.* Structure Control within Poly(amidoamine) Dendrimers: Size, Shape and Regio-Chemical Mimicry of Globular Proteins. **59**, 3799-3813 (2003).
144. Page, D. & Roy, R. Synthesis and biological properties of mannosylated starburst poly(amidoamine) dendrimers. *Bioconjugate Chem.* **8**, 714-723 (1997).
145. Dass, C. Vehicles for Oligonucleotide Delivery to Tumors. **54**, 3-27 (2002).
146. Smith, D. K. & Diederich, F. Functional Dendrimers: Unique Biological Mimics. **4**, 1353-1361 (1998).
147. Pagé, D. & Roy, R. Synthesis and Biological Properties of Mannosylated Starburst Poly(amidoamine) Dendrimers. **9**, 714-723 (1997).
148. Hong, M. Y. *et al.* Protein-Ligand Interactions at Poly(amidoamine) Dendrimer Monolayers on Gold. **19**, 416-421 (2003).
149. Yoo, H. & Juliano, R. L. Enhanced delivery of antisense oligonucleotides with fluorophore-conjugated PAMAM dendrimers. **28**, 4225-4231 (2000).
150. Shiwen, H. *et al.* Syntheses of Polyamidoamine Dendrimers Starting from a Hexadimensional Core and Application in Gene Transfer. **46**, 271-279 (2003).
151. Stiriba, S.-E. *et al.* Dendritic Polymers in Biomedical Applications: From Potential to Clinical Use in Diagnostics and Therapy. **41**, 1329-1334 (2002).
152. Denning, J. Gene Transfer in Eukaryotic Cells Using Activated Dendrimers. **228**, 227-236 (2003).
153. Patri, A. K. *et al.* Dendritic Polymer Macromolecular Carriers for Drug Delivery. **6**, 466-471 (2002).
154. Sato, N. *et al.* Tumor targeting and imaging of intraperitoneal tumors by use of antisense oligo-DNA complexed with dendrimers and/or avidin in mice. **7**, 3606-3612 (2001).
155. Kobayashi, H. *et al.* Comparison of Dendrimer-Based Macromolecular Contrast Agents for Dynamic Micro-Magnetic Resonance Lymphangiography. **50**, 758-766 (2003).
156. Kojima, C. *et al.* Design of Biocompatible Dendrimers with Environment Sensitivity. **36**, 2183-2186 (2003).
157. Kolhe, P. *et al.* Drug Complexation, in Vitro Release and Cellular Entry of Dendrimers and Hyperbranched Polymers. **259**, 143-160 (2003).
158. Röckendorf, N. & Lindhorst, T. K. Glycodendrimers. **217**, 201-238 (2001).
159. Veprek, P. & Jezek, J. Peptide and Glycopeptide Dendrimers. Part II. **5**, 203-220 (1999).
160. Aulenta, F. *et al.* Dendrimers: a New Class of Nanoscopic Containers and Delivery Devices. **39**, 1741-1771 (2003).
161. Krause, W. *et al.* Dendrimers in Diagnostic. **210**, 261-308 (2000).
162. Woller, E. K. & Cloninger, M. J. Mannose Functionalization of a Sixth Generation Dendrimer. **2**, 1052-1054 (2001).
163. Woller, E. K. & Cloninger, M. J. The Lectin-Binding Properties of Six Generations of Mannose-Functionalized Dendrimers. **4**, 7-10 (2002).
164. Woller, E. K. *et al.* Altering the Strength of Lectin Binding Interactions and Controlling the Amount of Lectin Clustering Using Mannose/Hydroxyl-Functionalized Denndrimers. **125**, 8820-8826 (2003).
165. Schlüter, A. D. & Rabe, J. P. Dendronized Polymers: Synthesis, Characterization, Assembly at Interfaces, and Manipulation. **39**, 864-883 (2000).
166. Kim, Y. & Zimmerman, S. C. Applications of Dendrimers in Bio-Organic Chemistry. **2**, 733-742 (1998).
167. Grayson, S. K. & Frechet, J. M. J. Convergent dendrons and dendrimers: from synthesis to applications. *Chem. Rev.* **101**, 3819-3867 (2001).
168. Ihre, H. R. *et al.* Polyester Dendritic Systems for Drug Delivery Applications: Design, Synthesis, and Characterization. **13**, 443-452 (2002).
169. Vutukuri, D. R. *et al.* Synthesis of Dendrimers with Multifunctional Periphery Using an ABB' Monomers. 796-797 (2003).
170. Sivanandan, K. *et al.* Functional Group Diversity in Dendrimers. **4**, 3751-3753 (2002).
171. Newkome, G. R. *et al.* Synthesis of New 1 -> (2 + 1) C-Branched Monomers for the Construction of Multifunctional Dendrimers. **36**, 4345-4354 (2003).
172. Cardona, C. M. *et al.* Dendrimer Functionalized with a Single Fluorescent Dansyl Group Attached "Off Center": Synthesis and Photophysical Studies. **122**, 6139-6144 (2000).
173. Chechik, V. & Crooks, R. M. Dendrimer-encapsulated Pd nanoparticles as fluorous phase- soluble catalysts. *J. Am. Chem. Soc.* **122**, 1243-1244 (2000).
174. Crooks, R. M. *et al.* in *Dendrimers Iii: Design, Dimension, Function* 81-135 (2001).
175. Niu, Y. H. *et al.* Size-selective hydrogenation of olefins by dendrimer- encapsulated palladium nanoparticles. *J. Am. Chem. Soc.* **123**, 6840-6846 (2001).
176. Sun, L. & Crooks, R. M. Interactions between dendrimers and charged probe molecules. 1. Theoretical methods for simulating proton and metal ion binding to symmetric polydentate ligands. *J. Phys. Chem. B* **106**, 5864-5872 (2002).
177. Zhao, M. Q. *et al.* Preparation of Cu nanoclusters within dendrimer templates. *J. Am. Chem. Soc.* **120**, 4877-4878 (1998).
178. Zhao, M. Q. & Crooks, R. M. Dendrimer-encapsulated Pt nanoparticles: Synthesis, characterization, and applications to catalysis. *Adv. Mater.* **11**, 217-+ (1999).
179. Zhao, M. Q. & Crooks, R. M. Homogeneous hydrogenation catalysis with monodisperse, dendrimer-encapsulated Pd and Pt nanoparticles. *Angew. Chem.-Int. Edit.* **38**, 364-366 (1999).

180. Zhou, L. *et al.* Characterization of poly(amidoamine) dendrimers and their complexes with Cu2+ by matrix-assisted laser desorption ionization mass spectrometry. *Macromolecules* **34**, 3567-3573 (2001).
181. Scott, R. W. J. *et al.* Synthesis, Charcaterization, and Stability of Dendrimer-Encapsulated Palladium Nanoparticles. **15**, 3873-3878 (2003).
182. Hecht, S. Functionalizing the Interior of Dendrimers: Synthetic Challenges and Applications. **41**, 1047-1058 (2003).
183. Majoros, I. J. *et al.* Acetylation of poly(amidoamine) dendrimers. **36**, 5526-5529 (2003).
184. Fail, C. A. *et al.* Controlled Attachment of PAMAM Dendrimers on Solid Support. **18**, 264-268 (2002).
185. Wang, Q. *et al.* Bioconjugation by copper(I)-catalyzed azide-alkyne 3+2 cycloaddition. **125**, 3192-3193 (2003).
186. Katritzky, A. R. & Singh, S. K. Synthesis of C-Carbamoyl-1,2,3-triazoles by Microwave-Induced 1,3-Dipolar Cycloaddition of Organic Azides to Acetylenic Amides. **67**, 9077-9079 (2002).
187. Speers, A. E. *et al.* Activity-based protein profiling in vivo using a copper(I)-catalyzed azide-alkyne 3+2 cycloaddition. **125**, 4686-4687 (2003).
188. Jeong, S. W. & O'Brien, D. F. Synthesis of a Polymerizable Metal-Ion-Chelating Lipid of Fluid Bilayers. **66**, 4799-4802 (2001).
189. Huynh, W. U. *et al.* CdSe nanocrystal rods/poly(3-hexylthiophene) composite photovoltaic devices. *Adv. Mater.* **11**, 923-+ (1999).
190. Alivisatos, A. P. Nanocrystals: Building blocks for modern materials design. *Endeavour* **21**, 56-60 (1997).
191. Klimov, V. I. *et al.* Mechanisms for intraband energy relaxation in semiconductor quantum dots: The role of electron-hole interactions. *Phys. Rev. B* **61**, R13349-R13352 (2000).
192. Yang, H. & Xie, X. S. Statistical approaches for probing single-molecule dynamics photon-by-photon. **284**, 423-437 (2002).
193. Yang, H. & Xie, X. S. Probing single-molecule dynamics photon by photon. **117**, 10965-10979 (2002).
194. Boon, J. M. & Smith, B. D. Synthetic membrane transporters. **6**, 749-756 (2002).
195. Fischer, P. M. *et al.* Cellular delivery of impermeable effector molecules in the form of conjugates with peptides capable of mediating membrane translocation. **12**, 825-841 (2001).
196. Garnett, M. C. Targeted drug conjugates: principles and progress. **53**, 171-216 (2001).
197. Hawiger, J. Noninvasive intracellular delivery of functional peptides and proteins. **3**, 89-94 (1999).
198. Lindgren, M. *et al.* Cell-penetrating peptides. **21**, 99-103 (2000).
199. Schwarze, S. R. *et al.* Protein transduction: unrestricted delivery into all cells? **10**, 290-295 (2000).
200. Schwarze, S. R. & Dowdy, S. F. In vivo protein transduction: intracellular delivery of biologically active proteins, compounds and DNA. **21**, 45-48 (2000).
201. Umezawa, N. *et al.* Translocation of a beta-peptide across cell membranes. **124**, 368-369 (2002).
202. Wender, P. A. *et al.* The design, synthesis, and evaluation of molecules that enable or enhance cellular uptake: Peptoid molecular transporters. **97**, 13003-13008 (2000).
203. Zelphati, O. *et al.* Intracellular delivery of proteins with a new lipid-mediated delivery system. **276**, 35103-35110 (2001).
204. Langel, U. (ed.) *Cell Penetrating Peptides* (CRC Press, Boca Raton, FL, 2002).
205. Cullis, P. M. *et al.* Chemical highlights of polyamine transport. **26**, 595-601 (1998).
206. Martin, S. E. & Peterson, B. R. Non-natural cell surface receptors: Synthetic peptides capped with N-cholesterylglycine efficiently deliver proteins into mammalian cells. **14**, 67-74 (2003).
207. Martin, S. E. & Peterson, B. R. Delivery of peptide-binding proteins into mammalian cells with synthetic cholesterylamine-terminated peptides. **41**, 8991-8991 (2002).
208. Hussey, S. L. & Peterson, B. R. Delivery of streptavidin-linked toxins to cancer cells with Streptaphage: protein uptake regulated by a membrane-anchored synthetic ligand. **41**, 8969-8969 (2002).
209. Hussey, S. L. & Peterson, B. R. Efficient delivery of streptavidin to mammalian cells: Clathrin-mediated endocytosis regulated by a synthetic ligand. **124**, 6265-6273 (2002).
210. Wang, C. J. *et al.* Molecular requirements for targeting the polyamine transport system. Synthesis and biological evaluation of polyamine-anthracene conjugates. **46**, 2672-2682 (2003).
211. Wang, C. J. *et al.* Synthesis and biological evaluation of N-1-(anthracen-9-ylmethyl)triamines as molecular recognition elements for the polyamine transporter. **46**, 2663-2671 (2003).
212. Haugland, R. P. *Handbook of Fluorescent Probes and Research Products* (Molecular Probes, Eugene, OR, 2002).
213. Rotman, B. & Papermaster, B. W. Membrane properties of living mammalian cells as studied by enzymatic hydrolysis of fluorogenic esters. **55**, 124-141 (1966).
214. Bierer, D. E. & Kabalka, G. W. Syntheses of w-alkynyl aldehydes and ketones via oxidation of w-alkynyl alcohols with pyridinium dichromate. **20**, 63-72 (1988).
215. Fawell, S. *et al.* Tat-Mediated Delivery of Heterologous Proteins into Cells. **91**, 664-668 (1994).
216. Bhorade, R. *et al.* Macrocyclic chelators with paramagnetic cations are internalized into mammalian cells via a HIV-tat derived membrane translocation peptide. **11**, 301-305 (2000).
217. Josephson, L. *et al.* High-efficiency intracellular magnetic labeling with novel superparamagnetic-tat peptide conjugates. **10**, 186-191 (1999).
218. Frankel, A. D. & Pabo, C. O. Cellular Uptake of the Tat Protein from Human Immunodeficiency Virus. **55**, 1189-1193 (1988).
219. Futaki, S. *et al.* Stearylated arginine-rich peptides: A new class of transfection systems. **12**, 1005-1011 (2001).

220. Mitchell, D. J. *et al.* Polyarginine enters cells more efficiently than other polycationic homopolymers. **56**, 318-325 (2000).
221. Rueping, M. *et al.* Cellular uptake studies with beta-peptides. **3**, 257-259 (2002).
222. Wright, L. R. *et al.* Guanidinium rich peptide transporters and drug delivery. **4**, 105-124 (2003).
223. Wender, P. A. *et al.* Oligocarbamate molecular transporters: Design, synthesis, and biological evaluation of a new class of transporters for drug delivery. **124**, 13382-13383 (2002).
224. Vives, E. *et al.* A truncated HIV-1 Tat protein basic domain rapidly translocates through the plasma membrane and accumulates in the cell nucleus. **272**, 16010-16017 (1997).
225. Derossi, D. *et al.* The 3rd Helix of the Antennapedia Homeodomain Translocates through Biological-Membranes. **269**, 10444-10450 (1994).
226. Polyakov, V. *et al.* Novel Tat-peptide chelates for direct transduction of technetium-99m and rhenium into human cells for imaging and radiotherapy. **11**, 762-771 (2000).
227. Testa, B. & Mayer, J. M. Design of intramolecularly activated prodrugs. **30**, 787-807 (1998).
228. Kirschberg, T. A. *et al.* Arginine-based molecular transporters: The synthesis and chemical evaluation of releasable taxol-transporter conjugates. **5**, 3459-3462 (2003).
229. Gerisch, G. & Muller-Taubenberger, A. in *Biophotonics, Pt B* 320-337 (2003).
230. Johnsson, N. & Johnsson, K. A fusion of disciplines: Chemical approaches to exploit fusion proteins for functional genomics. **4**, 803-810 (2003).
231. Keppler, A. *et al.* A general method for the covalent labeling of fusion proteins with small molecules in vivo. **21**, 86-89 (2003).
232. Gendreizig, S. *et al.* Covalent labeling of fusion proteins with chemical probes in living cells. **57**, 181-183 (2003).
233. Juillerat, A. *et al.* Directed evolution of O-6-alkylguanine-DNA alkyltransferase for efficient labeling of fusion proteins with small molecules in vivo. **10**, 313-317 (2003).
234. Felgner, P. L. *et al. Lipofection: a highly efficient, lipid-mediated DNA-transfection procedure* (1987).
235. Felgner, J. H. *et al.* in *J Biol Chem* 2550-61 (1994).
236. Zabner, J. *et al.* in *J Biol Chem* 18997-9007 (1995).
237. Lim, C. S. *et al.* Differential localization and activity of the A- and B-forms of the human progesterone receptor using green fluorescent protein chimeras. **13**, 366-375 (1999).
238. Tripp, B. C. *et al.* Investigation of the 'switch-epitope' concept with random peptide libraries displayed as thioredoxin loop fusions. **14**, 367-77 (2001).
239. Westerlund-Wikstrom, B. Peptide display on bacterial flagella: principles and applications. **290**, 223-30 (2000).
240. Lu, Z. *et al.* Expression of thioredoxin random peptide libraries on the Escherichia coli cell surface as functional fusions to flagellin: a system designed for exploring protein-protein interactions. **13**, 366-72 (1995).
241. Lu, Z. *et al.* Displaying libraries of conformationally constrained peptides on the surface of Escherichia coli as flagellin fusions. **87**, 265-80 (1998).
242. Liu, Q. *et al.* The univector plasmid-fusion system, a method for rapid construction of recombinant DNA without restriction enzymes. **8**, 1300-9 (1998).
243. Airenne, K. J. *et al.* Recombinant avidin and avidin-fusion proteins. **16**, 87-92 (1999).
244. Airenne, K. J. *et al.* Production of biologically active recombinant avidin in baculovirus-infected insect cells. **9**, 100-108 (1997).
245. Airenne, K. J. & Kulomaa, M. S. Rapid purification of recombinant proteins fused to chicken avidin. **167**, 63-68 (1995).
246. Airenne, K. J. *et al.* Production of Recombinant Avidin in Escherichia-Coli. **144**, 75-80 (1994).
247. Schwille, P. *et al.* Fluorescence correlation spectroscopy with single-molecule sensitivity on cell and model membranes. *Cytometry* **36**, 176-182 (1999).
248. Rigler, R. Fluorescence correlation spectroscopy and single molecule detection. *Biophys. J.* **74**, A4-A4 (1998).
249. Enderlein, J. & Kollner, M. Comparison between time-correlated single photon counting and fluorescence correlation spectroscopy in single molecule identification. *Bioimaging* **6**, 3-13 (1998).
250. Kinjo, M. *et al.* Single-molecule analysis of restriction DNA fragments using fluorescence correlation spectroscopy. *Anal. Biochem.* **260**, 166-172 (1998).
251. Haupts, U. *et al.* Dynamics of fluorescence fluctuations in green fluorescent protein observed by fluorescence correlation spectroscopy. *Proc. Natl. Acad. Sci. USA* **95**, 13573-13578 (1998).
252. Schwille, P. *et al.* Fluorescence correlation spectroscopy reveals fast optical excitation-driven intramolecular dynamics of yellow fluorescent proteins. *Proc. Natl. Acad. Sci. U. S. A.* **97**, 151-156 (2000).
253. Wu, M. M. *et al.* Organelle pH studies using targeted avidin and fluorescein-biotin. **7**, 197-209 (2000).
254. Hager, G. L. *et al.* Trafficking of nuclear receptors in living cells. **74**, 249-254 (2000).
255. Meyers, S. & Hiebert, S. W. Alterations in subnuclear trafficking of nuclear regulatory factors in acute leukemia. 93-98 (2000).
256. Stein, G. S. *et al.* Subnuclear organization and trafficking of regulatory proteins: Implications for biological control and cancer. 84-92 (2000).
257. Wu, M. M. *et al.* Mechanisms of pH regulation in the regulated secretory pathway. **276**, 33027-35 (2001).

258. Melvin, V. S. & Edwards, D. P. Expression and purification of recombinant human progesterone receptor in baculovirus and bacterial systems. **176**, 39-54 (2001).

259. Juuti-Uusitalo, K. *et al.* Selective targeting of avidin/mannose 6-phosphate receptor chimeras to early or late endosomes. **79**, 458-468 (2000).

Size-Dependent Au Nanodot Emission

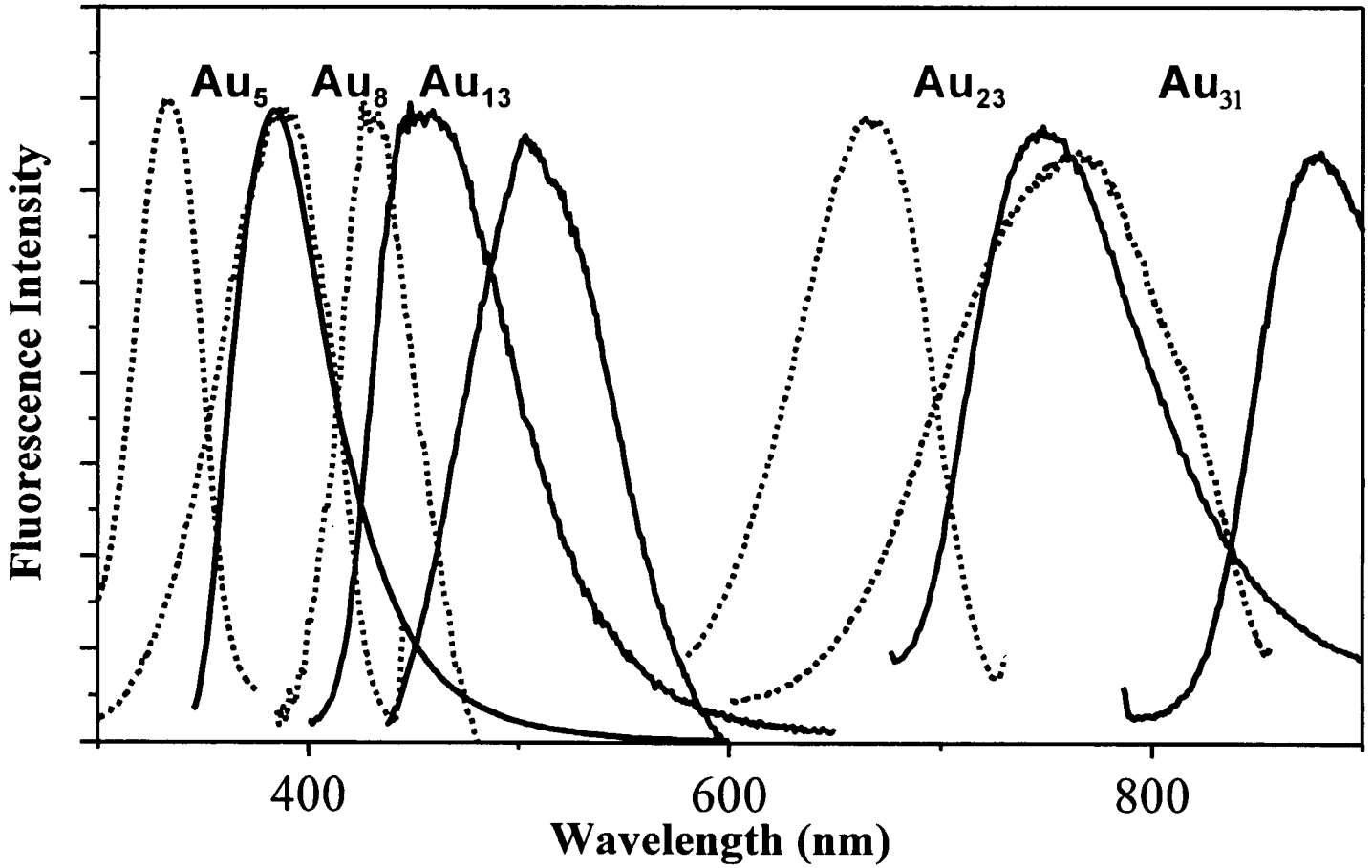

- Changing creation conditions affords tunability of discrete Au nanodot emission
- Emission energy scales with 1/(Cluster Radius)
- High concentration and spectrally pure samples readily created
- Size still relatively large (5-31 atoms)

WHAT IS CLAIMED:

1. An apparatus as described herein and as shown in the Figures, including each and every limitation and embodiment; and

2. A method of operation as described herein and as shown in the Figures, including each and every limitation and embodiment.